Northern Michigan University

NMU Commons

All NMU Master's Theses | Student Works

5-2014

HAPTIC AND EXOSKELETON DEVICES FOR NEUROREHABILITATION OF UPPER LIMB PARALYSIS: A STATE OF ART AND A NIGHT LANDING TASK

Samantha Renee Wagner
Northern Michigan University, samawagn@nmu.edu

Follow this and additional works at: https://commons.nmu.edu/theses

 Part of the Cognition and Perception Commons, and the Rehabilitation and Therapy Commons

Recommended Citation

Wagner, Samantha Renee, "HAPTIC AND EXOSKELETON DEVICES FOR NEUROREHABILITATION OF UPPER LIMB PARALYSIS: A STATE OF ART AND A NIGHT LANDING TASK" (2014). *All NMU Master's Theses*. 2.
https://commons.nmu.edu/theses/2

This Open Access is brought to you for free and open access by the Student Works at NMU Commons. It has been accepted for inclusion in All NMU Master's Theses by an authorized administrator of NMU Commons. For more information, please contact kmcdonou@nmu.edu,bsarjean@nmu.edu.

HAPTIC AND EXOSKELETON DEVICES FOR NEUROREHABILITATION OF UPPER LIMB PARALYSIS: A STATE OF ART AND A NIGHT LANDING TASK

By

Samantha Renee Wagner

THESIS

Submitted to
Northern Michigan University
In partial fulfillment of the Requirements
For the degree of

MASTER OF SCIENCE

Office of Graduate Education and Research

2014

SIGNATURE APPROVAL FORM

Title of Thesis: HAPTIC AND EXOSKELETON DEVICES FOR NEUROREHABILITATION OF UPPER LIMB PARALYSIS: A STATE OF ART AND A NIGHT LANDING TASK

This thesis by _____Samantha R. Wagner_____ is recommended for approval by the student's Thesis Committee and Department Head in the Department of _____Psychology_____ and by the Assistant Provost of Graduate Education and Research.

_____

Committee Chair: Dr. Mounia Ziat Date

_____

First Reader: Dr. Adam Prus Date

_____

Second Reader (if required): Dr. Scott Drum Date

_____

Department Head: Dr. Paul Andronis Date

_____

Dr. Brian D. Cherry Date
Assistant Provost of Graduate Education and Research

ABSTRACT

HAPTIC AND EXOSKELETON DEVICES FOR NEUROREHABILITATION OF UPPER LIMB PARALYSIS: A STATE OF ART AND A NIGHT LANDING TASK

By

Samantha Renee Wagner

Rehabilitation is an important training phase for those suffering from upper limb paralysis as a result of brain injury. When successfully completed, the re-trained limb should be able to successfully complete daily life activities. An alternative to traditional therapy is the usage of effective rehabilitation by using haptic devices in a virtual environment. The type of haptic device and task are crucial for the success of the therapy training sessions. After presenting a state-of-art literature review of several haptic devices that has been used in research and clinical facilities, we thought to use the black hole illusion (BHI), a night landing illusion, as a potential way to investigate the benefits of using a haptic device in a featureless environment. The purpose was to explore whether under a visual clueless environment, individuals could rely on their tactile and haptic modality to perform a task. More specifically, we asked the participants to land a virtual object during featured (F) and featureless night conditions (NF); with (H) and without haptic feedback (WH). The results showed that haptic feedback aided featureless night landing along the mediolateral direction. However, this benefit was less evident in a featured condition suggesting that participants were relying on visual cues during the task. This confirms previous findings related to night landing that the BHI is due to the fact that experienced pilots rely mainly on the visual input during the glide.

Copyright by

Samantha Renee Wagner

2014

ACKNOWLEDGMENTS

I would like to thank my thesis advisor Dr. Mounia Ziat and committee members Dr. Adam Prus and Dr. Scott Drum for all of their guidance and support throughout this project. Additional thanks for the NMU Psychology Department and to everyone in Dr. Ziat's Action and Perception Laboratory who have supported me throughout my time at Northern Michigan University. I would also like to thank all the students who participated in my study.

I would like to especially thank Matthew Pirkl, my friends, and family members for all of their invaluable support throughout my academic career.

TABLE OF CONTENTS

ACKNOWLEDGMENTS iii

LIST OF TABLES vi

LIST OF FIGURES viii

INTRODUCTION 1

CHAPTER ONE: HAPTIC AND EXOSKELETON DEVICES FOR NEUROREHABILITATION. 4

1. MOTOR PARALYSIS 4

1.1. CAUSES OF MOTOR PARALYSIS 4

1.2. Motor Recovery Assessments 6

2. Haptic and Exoskeleton devices 8

2.1. End-Effector Haptic Devices 8

2.2. Ungrounded Exoskeleton Robotic Devices 18

2.3. Grounded Exoskeleton Robotic Devices 24

3. RESEARCH STUDIES IN UPPER LIMB PARALYSIS 30

3.1. Studied Population 30

3.2. Types of Tasks 30

3.3. Participants' Performances 36

3.4. Conclusion 40

Chapter 2: A Night Landing Task Using a Haptic Feedback 44

1. Introduction 44

2. The Black Hole Illusion 44

3. Experiment 46
3.1. Participants 47
3.2. Apparatus and Stimuli 47
3.3. Procedure 48
3.4. Data Analysis 49
3.5. Results 49
4. Discussion 69
5. Conclusion 70
References 72
Appendix A: Python Scripts For Featured Haptics 83
Appendix B: Python Scripts for Featureless with Haptics 86
Appendix C: Instructions to Participants 88
Appendix D: Informed Consent Form 89
Appendix E: Excel File of Data Applied to Each Condition 92
Appendix F: Institutional Review Board Approval Form 93
Appendix G: Citi Module for Human Research Subjects 94

LIST OF TABLES

Table 1. Haptic and robotic devices used for neurorehabilitation. 11

Table 2. Studied Population in Neurorehabilitation 32

Table 3. KMO values for all participants for the x-axis (FH condition). Values for individual participants are highlighted in grey (significant > 0.5). 51

Table 4. KMO values for all participants for the y-axis (FH condition). Values for individual participants are highlighted in grey (significant > 0.5). 52

Table 5. KMO values for all participants for the z-axis (FH condition). Values for individual participants are highlighted in grey (significant > 0.5). 53

Table 6. KMO values for all participants for the x-axis (FWH condition). Values for individual participants are highlighted in grey (significant > 0.5). 55

Table 7. KMO values for all participants for the y-axis (FWH condition). Values for individual participants are highlighted in grey (significant > 0.5). 56

Table 8. Pearson correlation values; significant effects are shown by asterisks. 56

Table 9. KMO values for all participants for the x-axis (NFH condition). Values for individual participants are highlighted in grey (significant > 0.5). 58

Table 10. KMO values for all participants for the y-axis (NFH condition). Values for individual participants are highlighted in grey (significant > 0.5). 59

Table 11. KMO values for all participants for the z-axis (NFH condition). Values for individual participants are highlighted in grey (significant > 0.5). 60

Table 12. KMO values for all participants for the x-axis (NFWH condition). Values for individual participants are highlighted in grey (significant > 0.5). 62

Table 13. KMO values for all participants for the y-axis (NFWH condition). Values for individual participants are highlighted in grey (significant > 0.5). 63

Table 14. KMO values for all participants for the z-axis (NFWH condition). Values for individual participants are highlighted in grey (significant > 0.5). 64

Table 15. Pearson-r^2 values for x-axis (Significant =.4) 66

Table 16. Pearson-r^2 values for Y-axis beginning of Trajectory (Significant =.4). 67

Table 17. Pearson-r^2 values for Y-axis end of trajectory (Significant =.4). 67

Table 18. Pearson-r^2 values for z-axis (Significant =.4).....68

Table 19. Mean time values for each condition (FH, FWH, NFH, and NFWH). 69

LIST OF FIGURES

Figure 1. PHANToM OMNI (left) and PHANToM Desktop (from Geomagic Inc., 2013). 9

Figure 2. Premium 1.0 (top-left), Premium 1.5 (top right) and Premium 3.0 (From Geomagic inc., 2013).....10

Figure 3. Novint Falcon (from Nagaraj & Constantinescu, 2009). 12

Figure 4. MIT-Manus (right) and Hopkins Manipulandum (from Shadmehr & Brashers-Krug, 1997, & Krebs et al., 2005). 13

Figure 5. Mirror Imaging Motion Enabler (from Lum et al., 2002). 14

Figure 6. HapticMaster (from Van der Linde et al., 2002). 15

Figure 7. Adler with BiAs (left) and ACT-4D (from Johnson et al., 2011, & Steinen et al., 2011). 16

Figure 8. GENTLE/s system (left) and the GENTLE/g system (from Lourerio et al., 2001, & Lourerio et al., 2007).....17

Figure 9. PERCRO GRAB (from Bergamasco et al., 2006). 18

Figure 10. Cyber Grasp (a), CyberForce (b), CyberTouch (c), CyberGlove II (d), CyberGlove III (e) (from CyberGlove Systems LLC., 2012). 19

Figure 11. Rutgers Master II-ND (from Bouzit et al., 2002). 21

Figure 12. Body-Powered Orthosis (left) and Pneumatic-Powered Device (PPD) (from Luo et al., 2005). 22

Figure 13. HenRiE (from Podobnik, 2009). 23

Figure 14. BRAVO system (from Frisoli, 2009a). 23

Figure 15. HWARD (left) and L-Exos (right) (from Takahashi et al., 2005, & Frisoli, 2009a). 25

Figure 16. ARMin (from Nef et al., 2007). 26

Figure 17. MAHI Exo II (left) and RiceWrist (right) (from Gupta, & O'Malley, 2007; Pehlivan et al., 2011). 27

Figure 18. PureForm (from Frisoli, 2009a). 28

Figure 19. HIRO-III (from Hioki et al., 2011). 29

Figure 20. left) the horizon line in the actual environment, center) the environment as seen by the pilot does not contain as visual cues, except for the runway lights, right) the black hole illusion: the horizon line can be misperceived (from Watson, 1992). 45

Figure 21. Virtual runways for featured night (left) and featureless night (right) conditions. 48

Figure 22. Scree plots showing the inflection point (shown by the square) for a) x, b) y, and c) z directions for the FH condition. 51

Figure 23. Scree plots showing the inflection point (shown by the square) for a) x, and b) y directions for the FWH condition. 54

Figure 24. Scree plots showing the inflection point (shown by the square) for a) x, b) y, and c) z directions for the NFH condition. 57

Figure 25. Scree plots showing the inflection point (shown by the square) for a) x, b) y, and c) z directions for the NFWH condition. 61

Figure 26. Mean trajectory for each condition (FH, FWH, NFH, and NFWH) for x-axis. 65

Figure 27. Mean trajectory for each condition (FH, FWH, NFH, and NFWH) for y-axis. 67

Figure 28. Mean trajectory for each condition (FH, FWH, NFH, NFWH) for z-axis. 68

INTRODUCTION

In the past fifteen years, researchers have developed new ways to rehabilitate persons with motor deficiencies caused by damage to the nervous system (including spinal cord injury), stroke, cerebral palsy, or multiple sclerosis (Krakauer, 2005; Gupta & O'Malley, 2007; Loureiro, Harwin, Nagai, & Johnson, 2011; and Demain, Cunningham, Metcalf, Zheng, & Merrett, 2012). Besides drug prescriptions, persons with paralysis usually join an occupational therapy (OT) program. After each session, patients return back to their home environments and do not necessarily have the tools to function when trying to complete daily life activities (Krakauer, 2005), which might prevent full recovery of lost motor abilities. With the advancement of haptic and robotic technology, there may be more effective ways to rehabilitate individuals with lost motor functions. It can be combined with OT to not only regain motor functioning but also sensory abilities.

Haptic devices range from simple end-effector devices to full scale exoskeleton robots. They can be used with the hand or arm depending on what part of functioning is targeted (tactile, kinesthetic, or proprioceptive). This area of research has many future implications not only to advance neurorehabilitation of patients that suffer from a motor disability but also to understand the way humans interact with the world and their surrounding environment. The haptic and robotic devices that have been developed can provide a patient with motor deficiencies, a particular type of force feedback that usually gives an indication of the objects that are either in real or virtual environment.

The scope of chapter 1 focuses on the rehabilitation of the upper limbs, the different types of haptic devices, their usage in the neurorehabilitation, and their

implications in research. Chapter 1 starts first by describing the causes of motor paralysis and assessment methods used to determine the paralysis. We then described end-effector and exoskeleton devices separately and summarized the studied population, type of tasks, and performance outcomes followed by behavioral and neurophysiological evidence related to the usage of haptics in neurorehabilitation. We complete this chapter by discussing the implications of virtual environments and hybrid haptic devices that incorporate tactile or thermal inputs along with force feedback. This chapter is under review to be submitted to the journal IEEE Transactions on Haptics.

Chapter 2 discusses an experiment that incorporated virtual reality (VR) and a haptic device. Several tasks using virtual reality (VR) have been designed with haptic rehabilitation of upper limbs paralysis (more detailed in Chapter 1). Tasks usually vary from grasping simple objects to pick and place tasks, passing by pursuit, and trajectory tasks. For the scope of this thesis, we opted for a 3D trajectory task that consisted of landing an object on a target. Our experiment was inspired by a famous illusion in aviation known as the black hole illusion that affects pilots' final glide. This task could be a potential addition to the repertoire of tasks that already exists for rehabilitation. Not only does it include a 3D trajectory task, it also incorporates a pointing task, because the user is required to land the plan on a specific target. We encountered several technical and logistical issues during this phase. The first problem originated with the haptic device. Originally, we wanted to include both tactile and force feedback. However, the tactile display (two Braille cells) stopped working before running the experiment, which forced us to review our initial experiment that consisted of testing directional information improvements through tactile feedback. The second issue was related to the virtual

environment, whereby the programmer was unable to add runway lights to the landing strip and instead designed a vertical landing task rather than a conventional landing. Because of the timeline for the study and due to the confusion, he changed the part related to the type of landing (switching to conventional rather than vertical) and added a target on the runway to show a shooting point that ends the task. Adding the runway lights would have delayed the work by at least a month. Therefore, we decided to compare night landing in featured and featureless conditions by adding and removing the haptic feedback.

CHAPTER ONE: HAPTIC AND EXOSKELETON DEVICES FOR NEUROREHABILITATION

1. MOTOR PARALYSIS

1.1. CAUSES OF MOTOR PARALYSIS

By using their upper limbs, healthy individuals interact with objects using several ranges of movements (Pak & Pattern, 2008). A task such as grasping involves muscles of the arm and hand to orient or hold an object not only with a specific thumb and fingers arrangement, but also a precise force to avoid crushing or dropping the object. In such as a complex task, a person automatically determines the weight of the object and adjusts her grip accordingly. Individuals with motor paralysis might not necessarily be able to perform an automatic motor action to adjust their grip force or to make proper hand movements (Grunwald, 2008).

The major causes of motor paralysis are spinal cord injury (SCI), stroke, and traumatic brain injury (TBI). In the United States, over 15 million people suffer from strokes (National Stroke Association, 2014), 1.7 million individuals are affected by TBI (Centers for Disease Control and Prevention, 2012), and roughly 6 million are affected by paralysis in their upper and/or lower limbs as a result of spinal cord injury (SCI) (Reeve Foundation, 2013). Motor paralysis can also be due to multiple sclerosis (MS), cerebral palsy (Adamovich, Fluet, Tunik, & Merians, 2009), neurofibromatosis, and post-polio syndrome. Not necessarily leading to paralysis, but rather muscular dysfunction, other neurological condition affecting motor neurons such as Amyotrophic Lateral Sclerosis (ALS), or a group of muscles, such as focal dystonia, can also be debilitating when

performing everyday activities. The sufferer often has difficulty producing, controlling, and coordinating voluntary movements as characterized in cerebral palsy (Adamovich et al., 2009) or involuntary muscle movements as a result of continuing paralysis in ALS. Motor dysfunction could also be accompanied by cognitive deficiencies related to attention, memory, perception, or decision making (Tatemichi et al., 1994; & Reinkensmeyer, Emken, & Cramer, 2004).

In 60% of stroke patients the hand tends to be the most affected limb (Balascurbramanian, Klein, & Burdet, 2010). This might be related to the fact that a large portion of the sensorimotor cortex is allocated to the human hand (Balascurbamanian et al., 2010). The hand comes in contact with many aspects of the environment; it detects more information through tactile perception than any other part of the human body (Demain et al., 2012). It is also one of the hardest limbs to rehabilitate because of its complexity. Indeed, the human hand has 21 degrees of freedom (DOF), 15 joints, and 29 skeletal muscles that can be affected by damage to the motor or somatosensory (SM) cortices (Balascurbamanian et al., 2010, & Lum et al., 2012). Besides its complexity, it has very fine motor movements that are hard to replicate. If motor functions of the upper limbs are not addressed within the first three months and improvements are not seen by six months, a person may not be able to regain the level of motor skills she had before the stroke (Reinkensmeyer et al., 2004; McDonald & Sadowsky, 2004; & Krakauer, 2005).

Moreover spasticity is a feature that affects the stiffness of skeletal muscles and thus mobility and activities of daily life (ADL) (Miller et al., 2010) and is identified in 35% of stroke patients. Spasticity also occurs in MS, cerebral palsy, ALS, SCI, and TBI (Miller et al., 2010; & Reeve Foundation, 2013). Symptoms of spasticity often include

increased muscle tone, rapid muscle contractions, muscle spasms, and fixed joints; which could create deficiencies in limb range of motion, broken bones, infections, and sleep disorders (Reeve Foundation, 2013). Treatment of spasticity includes medication such as Baclofen, which targets reflexes that originate in the spinal cord. Physical therapy is also used to increase range of motion with the use of a brace (Reinkensmeyer et al., 2004; Miller et al., 2010; & Reeve Foundation, 2013). Pak and Patten (2008) claimed that neurorehabilitation therapy techniques that targeted strengthening muscles or repetition is often avoided because repetition could worsen spasticity.

When the paralysis is due to SCI, it is often difficult to determine the outcomes of rehabilitation due to the complexity and location of spinal injury. Indeed, a SCI can affect several outcomes of daily life such as depression, spastic reflex of the bladder and bowel movements, and decreased respiratory functioning, and arm pain from being wheelchair bound (Reeve Foundation, 2013). SCIs do not have to sever the spinal cord to affect functioning of motor movements or sensations. A bruised, stretched or crushed spinal cord can cause loss of limb functions (Reeve Foundation, 2013). Once a SCI is detected a person should receive proper treatment within 72 hours (McDonald & Sadowsky, 2004), otherwise recovery of lost motor functions could be hinder.

1.2. Motor Recovery Assessments

Physicians and therapists use several motor recovery assessments to determine the best treatment for the patients (Gladstone, Danells, & Black, 2002; & Rehabilitation Institute of Chicago, 2010). The Fugl-Meyer Assessment (FMA) of motor recovery after stroke is used to determine the level at which a person can function before and after treatment from a score of 0 (hemiplegic) to 100 (normal functioning). Usually five

aspects of human perception and motor functioning are tested: motor, sensory, balance, joint range of motion, and joint pain (Gladstone et al., 2002, & Rehabilitation Institute of Chicago, 2010). Similarly, the Chedoke Arm and Hand Activity Inventory (CAHAI) uses a 7 point scale evaluate functional recovery (CAHAI, 2004, & Cameirao, Badia, Duarte, Frisoli, & Verschure, 2012). For instance, a person who opened a jar without assistance receives a score of 7. One the other hand, a score of 1 is given if the person required assistance for the same task (CAHAI, 2004).

Barthel Index targets the performance of 10 ADLs such as feeding, bathing, grooming, dressing, bowel control, bladder control, toileting, chair transfers, ambulation, and stair climbing (Rehabilitation Institute of Chicago, 2010). These tasks are scored on a scale from 0 to 10; a score of 0 indicating the impossibility of completing the task, while a score of 10 indicates a total independence in task completion (The Internet Stroke Center, 2013).

The Jebson Hand Function Test allows the assessment of hand functions required for ADLs by having participants turn cards, pick up physical objects, write, and simulate feeding. A researcher or clinician observes the completion time of each task up to 120 seconds; a lower score denotes a higher level of motor functioning (Rehabilitation Institute of Chicago, 2010).

Finally, the Wolf Motor Function Test (WMFT) is used to assess the mobility of the upper limbs with 17 test items that take into account performance time, functional ability, and strength (Taub et al., 2011). Scoring for each task ranges from 0 (participant is not attempting to move her arm) to 5 (arm movement appears to be normal) (Rehabilitation Institute of Chicago, 2010).

Even though there are many different types of motor assessments, the most commonly used is FMA for its reliability, flexibility in assessing both upper and lower limb recovery, and high validity over the other types of assessments (Gladstone et al., 2002). Haptic neurorehabilitation research uses these assessments in combination with different haptic and robotic devices to determine how well a person improved upper limb functioning before and after completing a series of tasks.

2. HAPTIC AND EXOSKELETON DEVICES

The range of haptic and robotic devices used for rehabilitation is from simple gloves to full scale exoskeletons that fit over a person's entire arm. They are usually divided into two categories, end-effector and exoskeletons. Exoskeletons can be further sub-divided into ungrounded or grounded devices (Pehlivan, Lee, & O'Malley, 2012).

Table 1 summarized all devices discussed in this literature review. The use of an end-effector or exoskeleton device depends on the specific motor or cognitive deficiencies (Jack et al., 2001). Although these sub-categories will be described separately in the following sections, it is important to point out that they can be combined together (for instance, gloves can be combined with ungrounded exoskeletons or grounded exoskeletons). This type of interconnections, if any, will be mentioned when it is necessary.

2.1. END-EFFECTOR HAPTIC DEVICES

End-effectors are usually grounded haptic devices that allow interacting with the virtual or physical environment at the end of the device (Balascrubramanian et al., 2010; SensAble Technologies, 2012; & GeoMagic Inc., 2013). For neurorehabilitation of the

distal arm, several ADL tasks could be performed by adding specific tools or ungrounded exoskeletons to the end of the end-effector device.

FIGURE 1. PHANTOM OMNI (LEFT) AND PHANTOM DESKTOP (FROM GEOMAGIC INC., 2013).

One of the most popular end-effectors devices is the PHANToM manufactured by SensAble (currently Geomagic). The PHANToM Omni (Geomagic Touch) (Figure 1), the most affordable of the series, is a 6 DOF portable device that provides a force feedback workspace of 6.4W x 4.8H x 4.8D.

Similarly, the PHANToM Desktop (Geomagic Touch X) (Figure 1) is a 6 DOF with a larger workspace and provides a higher continuous exertable force. Both PHANToMs target hand movements pivoting at the wrist. The premium versions 1.0, 1.5, or a 3.0 (Figure 2) have 3 DOF of force feedback. Premium 1.0 targets the hand and wrist with a workspace of 10W x 7H x 5D. Premium 1.5 provides a user with workspace of 15W x 10.5H x 7.5D that targets elbow and lower arm movements. Finally, Premium 3.0 can potentially rehabilitate upper limb deficiencies that encompass the entire arm in a workspace of 33W x 23H x 16D. Different end effectors such as scissors or thumb pad could be used with the premium series. Theses series could also be offered with 6 DOF (SensAble Technologies, 2012; & GeoMagic Inc., 2013).

FIGURE 2. PREMIUM 1.0 (TOP-LEFT), PREMIUM 1.5 (TOP RIGHT) AND PREMIUM 3.0 (FROM GEOMAGIC INC., 2013).

TABLE 1. HAPTIC AND ROBOTIC DEVICES USED FOR NEUROREHABILITATION.

Type of Device	Haptic Device	Upper Limb Deficiency	Haptic Sense	Force Feedback Workspace	DOF (Joints)	# of Sensors	N
End- Effector	PHANToM OMNI	Hand: Pivot at the wrist	Kinesthetic	6.4W x 4.8H x 2.8D	6 (N/A)	N/A	3.3
	PHANToM Desktop			6.4W x 4.8H x 4.8D			7.9
	PHANToM Premium 1.0			10W x 7H x 5D			8.5
	PHANToM Premium 1.5/High Force	Lower arm movement		15W x 10.5H x 7.5D			8.5/37.5
	PHANToM Premium 3.0	Full Arm		33W x 23H x 12D			22
	Mit-Manus			N/A	2 -3	5	45-65
	Hopkins Manipulandum				2	N/A	N/A
	MIME				N/A		
	GRAB	Finger		300 x 400 x 600mm	6(N/A)	N/A	
	Novint Falcon	Lower arm movement		4 x 4 x 4	3		
	Haptic Master (Gentle/S, Gentle/G, Adler, Act-4D)	Arm		80·10-3 [m3]	3 (N/A)		100/250
Ungrounded Robotic	CyberGlove II	Hand and Fingers	Kinesthetic	1m spherical radius from actuator.	(N/A)	18/22	12
	CyberGlove III						
	CyberGrasp (Exoskeleton accessory to CyberGlove)					(N/A)	
	CyberForce (Exoskeleton accessory to CyberGlove)			12 x 12 in			8.8
	Cyber Touch(Exoskeleton accessory to CyberGlove)	Fingers	Tactile	3.0 x 4.55 x 1.04 in			1.2
	HenRiE (Glove)	Hand	Kinesthetic	N/A	3 (N/A)		90/100
	Rutgers Master II-ND (Glove)			2m radius hemisphere	5 (3)	4	16
	BPO/PPD			N/A	(2)	(N/A)	N/A
	BRAVEO				6 (5)	5	
Grounded Robotic	PURE-FORM	Fingers	Kinesthetic and Tactile	N/A	6 (N/A)	N/A	N/A
	HIRO-III		Kinesthetic	705 cm^3 (thumb) 587 cm^3 (other)	21 (21)	5	3.6
	HWARD	Wrist and hand		N/A	3 (N/A)	N/A	N/A
	RiceWrist	Forearm and wrist			4 (N/A)		
	MAHI	Wrist			N/A		
	ARMin	Shoulder and elbow			6 (N/A)		
	L-Exos				5 (6)		
	RGS: AREMO			2.7 m x 0.8 m x 1.65 m	6 (N/A)		

Another popular end-effector device that has been designed to incorporate different removable grips such as a pistol and a pen holder is the Novint Falcon (Figure 3) (Martin & Hillier, 2009). The Novint Falcon is a 3 DOF haptic device that was originally designed by Clavel (1990) for the gaming industry. With a 3D touch workspace of 4 x 4 x 4, the arm of this device can extend, retract and fold to measure the displacement in space which could be useful in pick and place tasks commonly used in neurorehabilitation research (Clavel, 1990; Martin & Hillier, 2009; & Nagaraj & Constantinescu, 2009).

FIGURE 3. NOVINT FALCON (FROM NAGARAJ & CONSTANTINESCU, 2009).

MIT-MANUS (Figure 4) was designed to provide the user with kinesthetic information by reducing friction to the arm and offers four different modules: three active for planar, vertical, and wrist movements and one passive for grasping (Krebs, Hogan, Edelstein, & Volpe, 1998; & Volpe et al., 2000). The active modules produce 2 to 3 DOF allowing easy movements while impedances provide 45N or 65N force feedback depending on the orientation of the handle (Krebs et al., 1998). Another device that is similar to the MIT-Manus, the Hopkins Manipulandum (Figure 4) is a 2 DOF portable device that is designed for the rehabilitation of the shoulder and elbow joints (Shadmehr & Brashers-Kruf, 1997).

FIGURE 4. MIT-MANUS (RIGHT) AND HOPKINS MANIPULANDUM (FROM SHADMEHR & BRASHERS-KRUG, 1997, & KREBS ET AL., 2005).

Finally, Mirror-Image Motion Enabler (MIME) (Figure 5) is a grounded haptic end-effector arm used for the rehabilitation of the upper extremities in stroke patients by imitating the movement of the non-affected limb (Gupta & O'Malley, 2007; Loureiro et al., 2011; & Tonelo, 2013). MIME can also be used for sign language communication or haptic guidance during exercising in healthy individuals (Tonelo, 2013). This device provides the operator with 6 DOF with unilateral and bimanual modes (Lum, Burgar, Shor, Majmundar, & Van der Loos, 2002; & Gupta & O'Malley, 2007) with three levels of resistance (passive, active-assisted, constrained). During the passive mode the robot moves the participants arm unlike in the active assisted mode where the patient moves her arm with the help of the device to reach the desired target. Finally during the constrained mode, MIME exerts resistance and forces the arm in a specific direction toward the goal. During the bilateral mode, mirror image movements of the non-affected arm are sent to the robot to guide the movements of the affected forearm which makes the only available system using the bilateral mode for rehabilitation of upper limb movements (Lum et al., 2005; & Tonelo, 2013).

FIGURE 5. MIRROR IMAGING MOTION ENABLER (FROM LUM ET AL., 2002).

Comparably, the HapticMaster (Figure 6) is a controlled end-effector device that uses the admittance control paradigm that consists of a force applied to the device by the user to obtain a proper reaction from the HapticMaster. This method has the advantage of being lightweight and backlash free (more friction at the joints level eliminated in a control loop), which allows smooth natural movements of the user (Van der Linde, Lammertse, Fredriksen, & Ruiter, 2002; Ziherl, Novak, Olensek, & Munih, 2010). With 3 DOF, it is possible to measure joint velocities of the hand within a vertical range of .40m and a pivot of 1 full radian (Van der Linde et al., 2002; Mihelj, Podobnik, & Munih, 2008; Verschuren, 2008; & Podobnik, Mihelj, & Munih, 2009). However, Verschuren (2008) suggested that the major limitation of this device is the non-realistic environment because of the generated friction, especially when the user is partaking in a task that requires motion with direction changes. To address this limitation, several friction models have been suggested to reduce the bump feeling effect felt by the user (Verschuren, 2008). HapticMaster can be enhanced with a number of accessories for different rehabilitation applications that will be discussed later in this manuscript.

FIGURE 6. HAPTICMASTER (FROM VAN DER LINDE ET AL., 2002).

HapticMaster has been used for several therapy environments such as the Activities of Daily Life Robot (ADLER), Arm Coordination Training 3D (ACT-3D), and ACT-4D (Figure 7) (Sukal, Ellis, & Dewald, 2006, Wisneski & Johnson, 2008, Johnson, Lourerio, & Harwin, 2008, & Stienen, McPherson, Schouten, & Dewald, 2011). ADLER combines HapticMaster with a hand orthotic to create functional grasp and reaching movements when manipulating virtual and real objects. ADLER has been used with a bilateral assessment system (BiAS) that measure left and right arm movements before, during, and after ADLER tasks (Wisneski & Johnson, 2008; & Johnson et al., 2008). The BiAS system has the advantage of being low cost to facilitate its transferability to home treatment option (Johnson et al., 2011). ADLER has also been used in collaborative tele-rehabilitation to facilitate semi-autonomous exercises (Johnson et al., 2008). In contrast, the ACT-3D system includes a HapticMaster combined with a Biodex experimental chair as a base for a 6 DOF device that can measure specific impairments by manipulating gravitational forces in a virtual environment within a workspace of 400 x 400 x 400mm (Sukal et al, 2006).

Similarly, ACT-4D, a modified version of the ACT-3D, is a 4 DOF device that adds an elbow rotation mechanism that stretches the muscles around the elbow. The system uses a 16 channel EMG to record muscle activity (Stienen et al., 2011). ACT-4D allows to either between admittance and direct controls which consists of controlling the position and the speed either based on the user output (admittance) or predefined profiles (Stienen et al., 2011).

FIGURE 7. ADLER WITH BIAS (LEFT) AND ACT-4D (FROM JOHNSON ET AL., 2011, & STEINEN ET AL., 2011).

Hapticmaster was also combined with a glove-like robotic wrist and grasping device to produce the Gentle/G (Grasp Robotic Exoskeleton) (Figure 8). The Gentle/S project was developed to evaluate therapies that combine virtual reality and haptics. It can be used in a variety of tasks that aim errorless learning and targets intensive neurological and physical rehabilitation in stroke patients by using repetitive movements in a virtual environment. Along with repetitive movements, this device also provides patients with visual, kinesthetic, and force feedback (Loureriro, Amirabdollahian, Coote, Stokes, & Harwin, 2001; Loureriro, Amirabdollahian, Topping, & Harwin, 2009). In comparison, Gentle/G, an extension of Gentle/S, is a 9 DOF robotic device that can

simulate hand movements during the interaction with a virtual setting. Being composed of the HapticMaster, an elbow orthotic and a key pad, it can be used in a variety of different virtual scenarios that promote ADLs and that involve reaching and grasping objects in a life-like or game environment. This 44N and three joints system could be used for rehabilitation of patients suffering of hemiparesis (Loureriro & Harwin, 2007; & Loureriro, Lamperd, Collin, & Harwin, 2009).

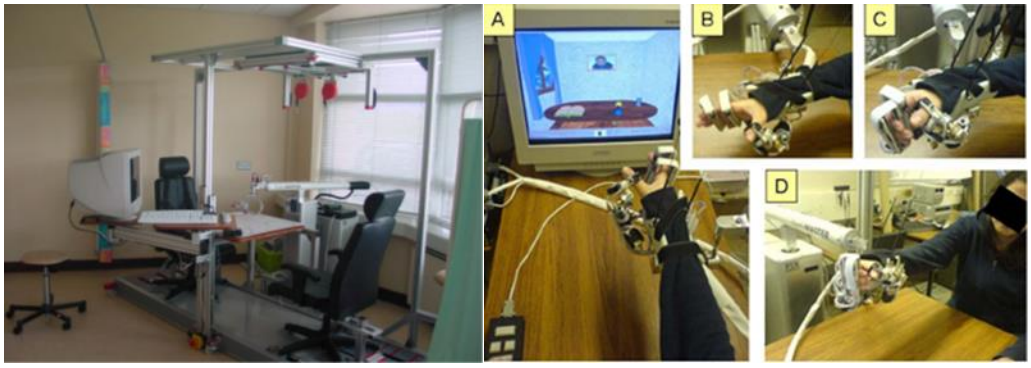

FIGURE 8. GENTLE/S SYSTEM (LEFT) AND THE GENTLE/G SYSTEM (FROM LOURERIO ET AL., 2001, & LOURERIO ET AL., 2007).

PERCRO GRAB (Figure 9) is a grounded haptic device that has two arms and provides force feedback to each index finger placed in thimbles. Each of the two arms has 6 DOF (3 DOF for position tracking and 3 DOF for finger orientation. Each of the two hands to be positioned in front of each other to allow participants to interact and manipulate virtual objects in a large workspace (300 x 400 x 600mm) (Bergamasco, Avizzano, Frisoli, Ruffaldi, & Marcheschi, 2006). GRAB has been used in conjunction with a rehabilitation gaming system (RGS) and ARMEO/T-Rex (Sanchez et al., 2006), an exoskeleton, in motor recovery in stroke patients in a virtual task (Cameiro et al., 2012).

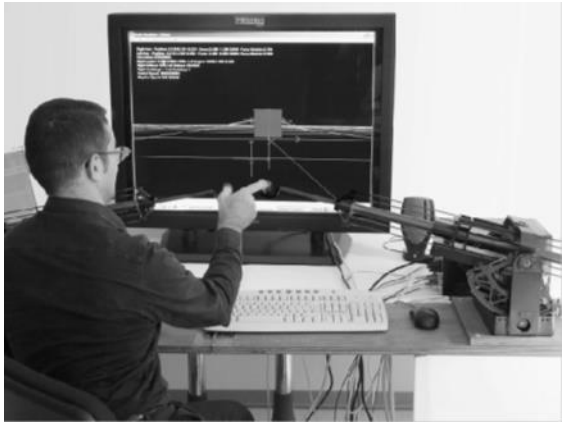

FIGURE 9. PERCRO GRAB (FROM BERGAMASCO ET AL., 2006).

The end-effector devices allow the interaction in both physical and virtual environments. Their DOF vary from 2 to 6 and could be used for neurorehabilitation of upper limb paralysis. Their usage is generally limited to grasping or strength tasks by adding accessories at the end of the effector. Ungrounded exoskeleton devices (described below) can often be combined with end-effectors to study different aspects of movement such as fine motor skills and are as efficient by themselves because they can be worn by the user for a larger range of motion for grasp, grip strength movements.

2.2. UNGROUNDED EXOSKELETON ROBOTIC DEVICES

Devices that are not attached to an external frame of reference are known as ungrounded robotic devices. Exoskeletons are usually worn by the individual to assist the limb movements. The CyberGrasp (Figure 10a) is a light weight exoskeleton that could be attached to the CyberGlove series to provide force feedback to the fingers and hand and could be used in VR to manipulate 3 dimensional (3D) objects. The grasp force feedback on each finger can be provided by five adjustable actuators to prevent crushing virtual objects (CyberGlove Systems, 2012). The user experiences a continuous 12N

force and has a usable workspace of one meter within a circular radius. By attaching CyberForce (Figure 10b), a force feedback armature, to CyberGrasp, a virtual steering wheel is created in a workspace of 12 x 12 inches with a force of 8.8 N and where the hand is hanged in the virtual space (CyberGlove Systems, 2012).

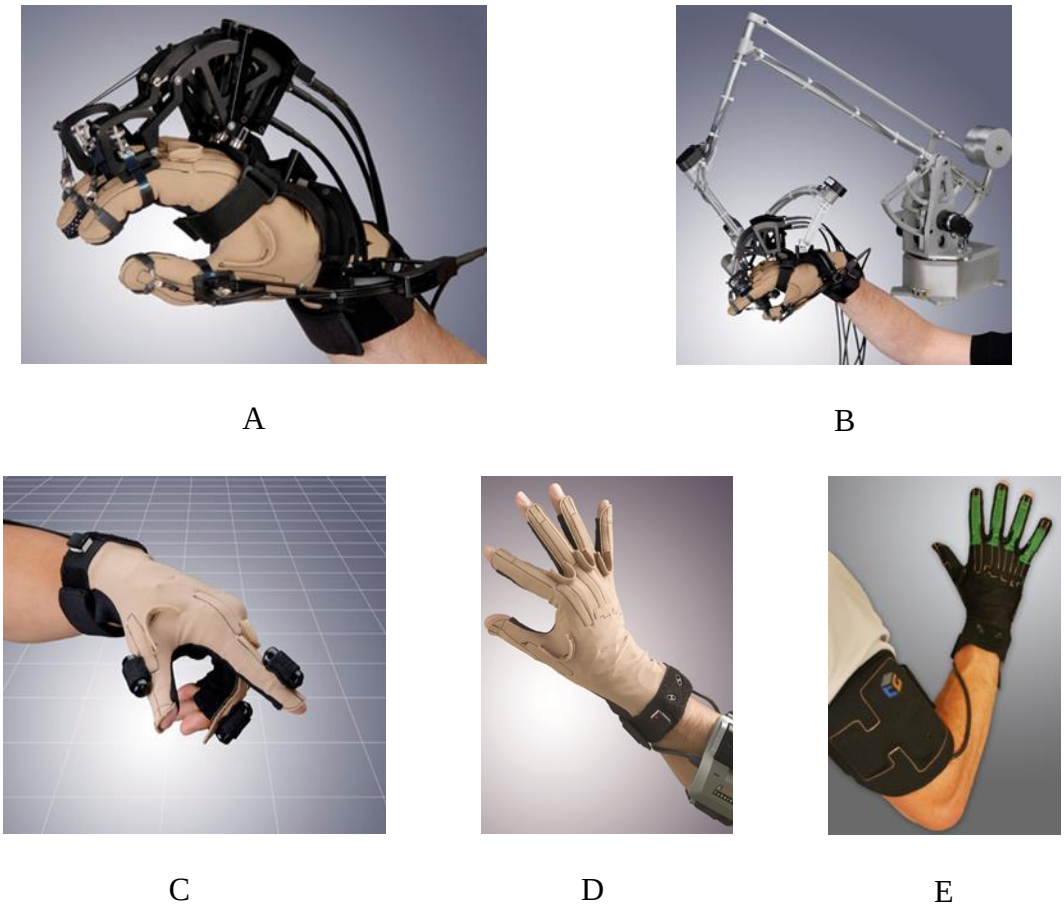

A B C D E

FIGURE 10. CYBER GRASP (A), CYBERFORCE (B), CYBERTOUCH (C), CYBERGLOVE II (D), CYBERGLOVE III (E) (FROM CYBERGLOVE SYSTEMS LLC., 2012).

In order to feel textures CyberTouch (Figure 10c), that could be an optional feature to CyberGlove, consists of 6 vibrotactile actuators, one located on each finger that could provide up to 1.2N. The vibrotactile feedback can simulate water-like content, magnetic field strength, light intensity, and the sensation of fluid moving across the hand (CyberGlove Systems, 2012). CyberGlove II (Figure 10d) and III (Figure 10e) are the

most popular and provide up to 18 or 22 sensors that encompass the entire hand and detect movements at 90 records per second. CyberGlove III has the advantage over CyberGlove II of providing a Wi-Fi connection which allows the participant to be up to 100 feet away from an internet source and thus offers a better maneuverability (CyberGlove Systems, 2012).

Rutgers Master II-ND (RMII) (Figure 11) is another exoskeleton glove that has been compared to and used in conjunction with CyberGlove and CyberGrasp. RMII-ND provides a force of 16 N and a 100 psi of air can be provided to each of the actuators on the fingers (Jack et al., 2001; & Bouzit, Popescu, Burdea, & Boian, 2002). RMII-ND differs from CyberGrasp in the infrared sensors included on it that measure fingertip displacement based on flexion and abduction in its multi-layer design with 4 DOF and four joints that makes dexterous movement possible in a virtual environment (Jack et al., 2001; & Bouzit et al., 2002). Even though the RMII-ND and CyberGrasp system are fairly similar in terms of capabilities, their design is quite different. Indeed the actuators are placed on the dorsal side and therefore hinder the full closing of the hand while the placement of the actuators on Cybergrasp are on the dorsal side. However, RMII-ND is lighter than the CyberGrasp and its sensors update rate is 435 records per second compared to 112 records per second of the CyberGrasp, which results in a faster reading. Finally, these devices also differ in the continuous force feedback that can be experienced by each finger as well as other properties such as sensors resolution, actuator type, or the workspace (for a full comparison see Bouzit et al., 2002).

FIGURE 11. RUTGERS MASTER II-ND (FROM BOUZIT ET AL., 2002).

When it comes to rehabilitating post-stroke patients, Luo et al. (2005) suggested a glove that is attached to two devices, the Body Powered Orthosis (BPO) and the Pneumatic-Powered Device (PPD) (Figure 12) to overcome the limitations experienced by the CyberGrasp (weight and cost) and RMII-ND (non-stereo display known as a fish tank VR, and grasping simulation due the limited flexion angle). The BPO is fixed on the shoulder and is connected to the hand by cables while the PPD uses an air balloon located in the palmar area that inflates and deflates to help finger extension exercises (Luo et al., 2005). This combined system has the advantage of being lightweight, being interfaced with an augmented reality environment, providing assistance when voluntary movements are detected, and allowing the therapist to monitor the session through visual, audio, and haptic stimulation (Luo et al., 2005; & Luo, Kenyon, & Kamper, 2006).

FIGURE 12. BODY-POWERED ORTHOSIS (LEFT) AND PNEUMATIC-POWERED DEVICE (PPD) (FROM LUO ET AL., 2005).

A prototype glove device that is making its way into the realm of neurorehabilitation and haptic research is HenRiE (Haptic environment for reaching and grasping exercises) (Figure 13), that has been shown to be successful in the rehabilitation of stroke patients with motor deficits by re-training grip movements with the use of two single axis cells positioned between the fingers (Mihelj et al., 2008; & Podobnik et al., 2009). Including 3 DOF and up to a maximum force of 90 to 100N, HenRiE assists user hand movements and was designed for grasping tasks in a virtual environment that focuses on proximal and distal movements of the upper extremities (Mihelj et al., 2008; & Podobnik et al., 2009). This is achieved by using HapticMaster, a grounded end-effector device that was described in the previous section.

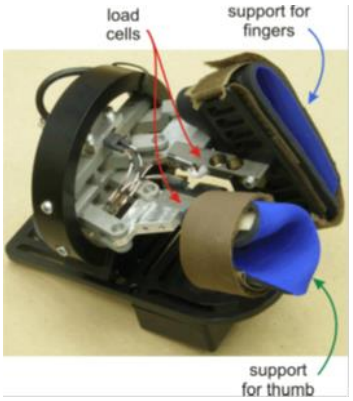

FIGURE 13. HENRIE (FROM PODOBNIK, 2009).

Finally, Loconsole et al. 2013 combined BRAVO, an ungrounded exoskeleton orthotic glove with an EMG to target bilateral hand movements. The BRAVO system (Figure 14) allows the control and the modulation of circular grasping tasks in post-stroke patients (Loconsole et al. 2013).

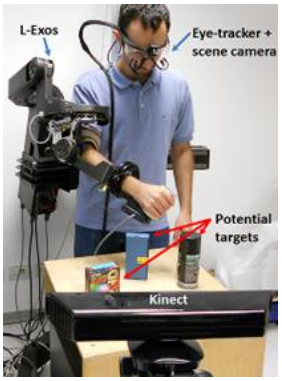

FIGURE 14. BRAVO SYSTEM (FROM FRISOLI, 2009A).

Ungrounded exoskeleton devices discussed in this section are remarkable in terms of rehabilitation since they could focus on specific functions of the hand. They can be combined with grounded end-effectors to target the entire arm and increase the range of movements and for rehabilitation. They have the advantage of encompassing the fingers

and are not limited to the wrist as it is the case with end-effectors devices. However, their limitation is that they only focus on motor functions relating to the hand and do target entire upper limb functioning as it is the case with grounded exoskeleton devices.

2.3. GROUNDED EXOSKELETON ROBOTIC DEVICES

Robotic devices that have an external mechanism that allows them to be freestanding are known as grounded. Exoskeletons tend to be full scale robotic devices that support the entire arm and hand. They have the advantage of being adaptable to the type of upper limb deficiency in terms of fit, length, and comfort (Gupta & O'Malley, 2007). The customization of grounded robotic devices can target hand sizes (Merians et al., 2002; Takahashi, Der-Yeghiaian, & Cramer, 2005; & Sledd & O'Malley, 2006), finger angles (Boian et al., 2002; Broeren, Rydmark & Sunnerhagen, 2004; Broeren, Rydmark Bjorkdahl, & Sunnerhagen, 2007), and affected limb arm length (Boian et al., 2002, Loureiro et al., 2011; & Pehlivan et al., 2012) to facilitate task completion; a feature that is often missing in end-effector devices and some ungrounded exoskeletons.

The Hand Wrist Assisting Robotic Device, HWARD, (Figure 15), is a 3 DOF robotic device that helps individuals improve different aspects of grasp and produces up to 122.8 N of force. An interesting feature of this device is backdriveability that provides the participant the ability to move the device while in a passive state, which has the advantage of not restricting hand movements. Besides, HWARD can be customized to adapt each person's hand. In terms of rehabilitation, HWARD offers ideal conditions that focus on the kinematics of the hand and wrist by assisting patients grasp either real or virtual objects with their deficient upper arm (Takahashi et al., 2005).

Another exoskeleton that also allows customization is the PECRO L-Exos (Figure 15), which can produce a force of 100N on the user's palm. L-Exos has 5 DOF, four of which are actuated for end-effector positioning which allows several joint configurations; while the fifth passive DOF allows free wrist movements. Each one of the 5 DOF could tar-get a specific portion of the arm, for instance the first joint focuses on the shoulder, while the other four target the elbow, forearm, and wrist/palm of the hand (Frisoli et al., 2008). The flexibility of L-Exos resides in the fact that it can be adapted to the length of the persons' arm which allows for a more comfortable training period that can properly target an upper limb dysfunction. It can also be used as a "hybrid bionic system" when combing eye gaze tracking to complete tasks that involve picking and placing items (Lonconsole et al., 2011).

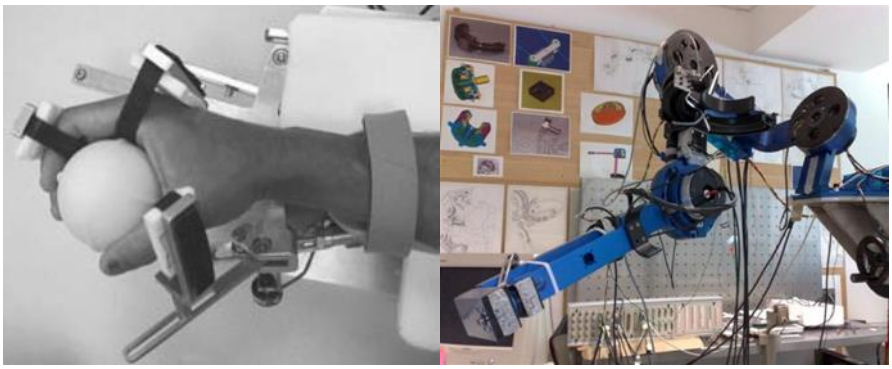

FIGURE 15. HWARD (LEFT) AND L-EXOS (RIGHT) (FROM TAKAHASHI ET AL., 2005, & FRISOLI, 2009A).

ARMin (known as ARMEO/T-REX) (Figure 16), a 6 DOF (4 active, 2 passive) grounded semi-exoskeleton, targets the rehabilitation of the entire arm, which is placed in an orthotic shell and can be used interchangeably between the right and left limbs. This interchangeable is an important feature that was missing in previously cited devices (Nef,

Mihelj, & Riener, 2007; Loureiro et al., 2011; Guidali et al., 2011). It can be adjusted to various levels of upper limb paralysis. For instance, a person can voluntarily move her arm to a specific target without any assistance or be guided by ARMin when movement is not detected (Nef et al., 2007; & Guidali et al., 2011).

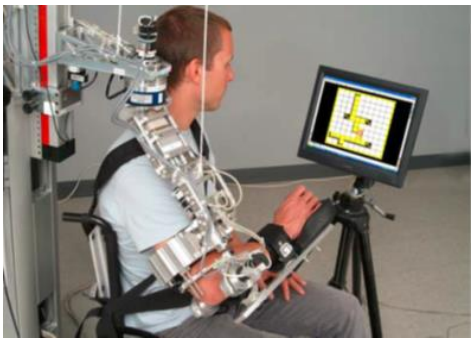

FIGURE 16. ARMIN (FROM NEF ET AL., 2007).

The Rice MAHI Exo II (Figure 17) can be used in a virtual reality environment for the rehabilitation of stroke, spinal cord injuries, or individuals who lack strength in their arms or wrists (Sledd & O'Malley, 2006; & Gupta & O'Malley, 2007). MAHI Exo II has five joints (5 DOF), one at the forearm, elbow, and three at the wrist. Its workspace is almost identical to a humans' range of motion (flexion: 0-90 degrees; extension 0-70; abduction 0-25, and adduction 0-65 (The Merck Manual, 2013) within the joints due to the 3 revolute-prismatic-spherical (RPS) platform (Gupta & O'Malley, 2007). It also accommodates varying hand sizes as well as bicep sizes through adjustable straps (Sledd & O'Malley, 2006). The MAHI Exo II and the MIME (mentioned under section 3.1) can be integrated together to form a device known as the RiceWrist.

The RiceWrist (Figure 17), a grounded forearm haptic exoskeleton, was designed to improve hand dysfunction by targeting the wrist and the forearm (Gupta & O'Malley,

2007). It has 3 DOF that has a revolute forearm joints and 3 revolute prismatic spherical (RPS) platform directed to target wrist motion. The platform and forearm joints, along with the inverse kinematics allow the user to reproduce natural movements including forearm rotation (O'Malley et al., 2006; & Pehlivan, Celik, & O'Malley, 2011). It is possible to control the force feedback and it is possible to combine RiceWrist with virtual environments that could enhance the rehabilitation process of a person with a motor deficit. Three possible modes: passive, active-assisted, and constrained modes are operational. When the RiceWrist is in the passive mode, the user does not control the exoskeleton, as RiceWrist guides the participant to the predetermined goal; while in the active mode the movement is controlled by the user. The active-assisted mode does not allow the robotic to assist the patient until it reaches a certain pre-programed threshold. This constrained mode allows the patients to actively move their arm to a desired position where RiceWrist delivers resistance to certain movements. Research with RiceWrist is still in progress to incorporate other aspects of arm movements (Gupta & O'Malley, 2007; & Pehlivan et al., 2011).

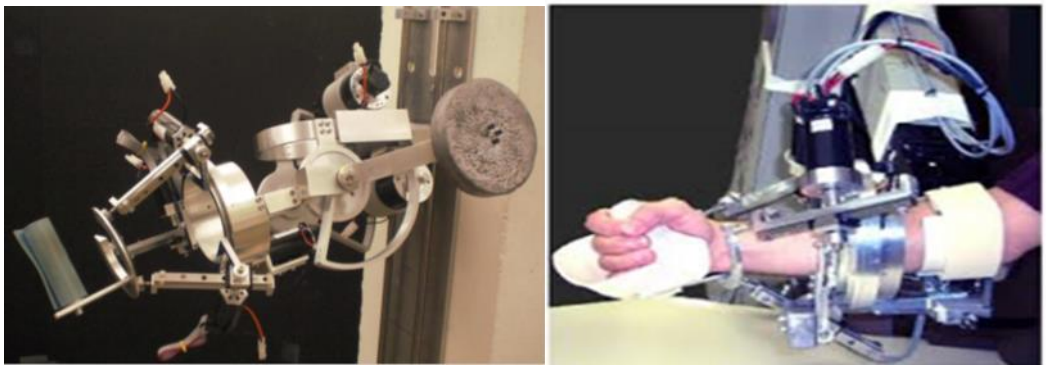

FIGURE 17. MAHI EXO II (LEFT) AND RICEWRIST (RIGHT) (FROM GUPTA, & O'MALLEY, 2007; PEHLIVAN ET AL., 2011).

In contrast, the PURE-FORM (Figure 18) is a 6 DOF, haptic exoskeleton device designed for the hand that delivers force feedback to thumb and index fingers (Frisoli, Bergmamasco, Wu, & Ruffaldi, 2005; & Frisoli et al., 2011). The principal is similar to the end-effector system GRAB in terms of contact points; however, the difference resides in the fact that PURE-FORM is worn around the hand and is usually combined with an arm exoskeleton (Frisoli, 2009a). Interestingly, this device has being used in a virtual museum project to explore and create 3D art, sculpture, and perceive with haptic feedback (Pure Form, 2004).

FIGURE 18. PUREFORM (FROM FRISOLI, 2009A).

Another device that focuses on the rehabilitation of the hand, specifically the fingers is HIRO-III (Figure 19). This multi-fingered haptic robot includes five small metal balls that points on the fingertips. The actuated motors allow a patient to partake in finger exercises by producing a high precision three direction force to the fingers. HIRO-III has 3 joints within each finger and 6 joints on the robotic arm which produces 21 DOF (15 DOF for the hand with 6 DOF for the interface arm). Each of the robotic joints looked at different aspect of human movement such as abduction-adduction and flexion-

extension (Endo et al., 2011). HIRO-III can produce up 3.6 N maximum on each fingertip. A biofeedback interface can be used to measure the muscular contraction that could indicate a participant's intentional movement and al-lows for the identification of affected muscles in case of an injury. The biofeedback is created by the use of a surface Electromyogram (sEMG) and delivers force feed-back accordingly (Hioki et al., 2004).

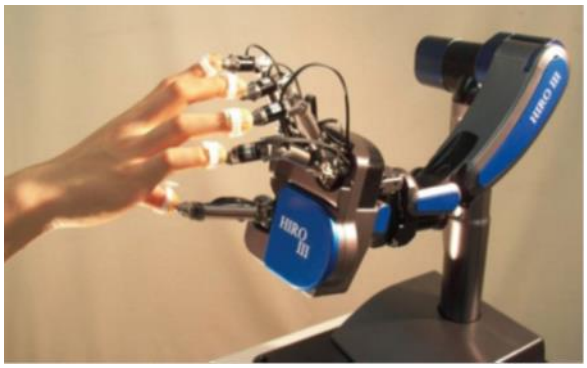

FIGURE 19. HIRO-III (FROM HIOKI ET AL., 2011).

In summary, grounded exoskeletons are highly effective in the rehabilitation of upper limb paralysis because they target the whole arm, including the fingers. They can be applied to multiple joints as it is the case with L-Exos, ARMin, and RiceWrist. This flexibility allows researchers to investigate rehabilitation of fine motor control and a larger range of motion. Despites the fact that grounded exoskeleton devices produced higher forces and have higher DOFs than ungrounded exoskeletons, they cannot be used in an in home setting. The patient has to travel to research or clinical facility for the training sessions.

3. RESEARCH STUDIES IN UPPER LIMB PARALYSIS

3.1. STUDIED POPULATION

Table 2 summarizes the studied population in neurorehabilitation research, whether they suffered from upper limb paralysis, and the type of tasks and haptic devices used. Many of the devices discussed previously have been tested with healthy individuals (Lum et al., 2002), (Frisoli et al., 2005; Sledd & O'Malley, 2006; O'Malley et al., 2006; & Frisoli et al., 2011) to establish a baseline by determining the level of non-deficient functioning, which later could be compared to individuals with motor deficiencies. When devices are not being used as a baseline, stroke patients are commonly tested in research or clinical facilities with end-effector and exoskeleton devices to demonstrate not only the usefulness of these devices, but also to determine what device features could be improved to facilitate the rehabilitation of upper limbs (Lum et al., 2002; Gupta & O'Malley, 2006; Loureiro et al., 2009; & Loureiro et al., 2011). However, stroke patients tend to be used in small numbers and their training could take several months or years after they experienced the initial stroke (Broeren et al., 2004; & Broeren et al., 2007).

3.2. TYPES OF TASKS

Tasks that target aspects of daily functioning such as grasping or pick-and-place objects were tested using CyberGloves, HenRiE, and RMII; while customized tasks to the individual's specific needs were used with the grounded exoskeleton devices described in Section 3.3. For instance, Guidali et al. (2011) has demonstrated how ARMin can be adjusted to individual needs using virtual reaching exercises and can be adapted to the patient's range of motion.

The PHANToM has been used in several different types of tasks such as brick and block game (Broeren et al., 2004; & Broeren et al., 2007); block and ball task in TBI patients (Reiner et al., 2004); pursuit tasks to increase attention (Dvorkin et al., 2009; Rozario et al., 2009; Larson et al., 2011) or maze navigation (Jarillo-Silva, Dominguez, & Parra-Vega, 2010). With movement being a concern in TBI and stroke patients, other cognitive problems related to memory can arise. Jarilla-Silva et al. (2010) presented a plausible method to measure learning performances related to kinesthetic memory in healthy subjects by using PHANToM 1.0 in maze navigation task that can be practice in a patient's home.

TABLE 2. STUDIED POPULATION IN NEUROREHABILITATION

Reference	Type of Brain Injury	Hemisphere Affected	Motor/Cognitive Deficiency	Task	Device Used	Assessments
Boian et al., 02	Stroke	Right	Hand Functions	Range of Motion, Speed of Motion, Fractionation	CyberGlove, RMII-ND	Jebsen Test of Hand Function
Broeren et al., 04, 07	Contralateral Stroke	Left, Right	Wrist	Ball & Block	PHANToM	Box and Block Test, AMPS
Cameirao et al., 12	Stroke	Left, Right	Upper Limb	Sphere grasping	RGS/GRAB/ARMEO	Motricity Index, Modified Ashworth Scale, FMA, CAHAI
Dvorkin et al., 09	TBI, Healthy	N/A	Upper Limb/ Attention	Location of spheres	PHANToM 3.0	N/A
Finley et al., 05	Stroke	Left, Right	Upper Limb	Reaching	MIT-Manus	WMFT, FMA Motor Power Assessment
Frisoli et al., 09	Stroke	N/A	Arm	Grasp, path following & Reach	L-Exos	N/A
Frisoli et al., 11	Healthy	N/A	Fingers/ Tactile Perception	Object Identification	PURE-FORM	N/A
Guidali et al., 11	Healthy, Stroke	N/A	Upper Limb/ Attention & Vision	Grasp & Reach	ARMin	FMA
Hioki et al., 11	Healthy	N/A	Finger	Open hand & Pinch Fingers	HIRO-III	N/A
Jack et al., 01	Stroke	Left	Hand Functions	Range of Motion, Finger Fractionation, & Strength	CyberGlove, RMII	Jebsen Test of Hand Function FMA
Jarilla-Silva et al., 10	Healthy	N/A	Upper Limb/ Attention	Maze Completion	PHANToM 1.0	N/A
Krebs et al., 04	Stroke	N/A	Upper Limb	Shoulder and elbow planar therapy	MIT-Manus	N/A
Johnson et al., 08	Healthy	N/A	Upper Limb	Reaching and Grasping.	Adler, Gentle/S, HapticMaster	N/A
Larson et al., 11	TBI	N/A	Upper Limb/ Attention	Location of Spheres	PHANToM	N/A
Lonconsole et al., 13	Healthy	N/A	Hand and Finger	Bilateral Grasping	BRAVO	N/A
Loureiro et al., 01	Healthy	N/A	Upper Limb/Attention	Grasping and Reaching of Virtual and Real-Life Objects	Gentle/S, HapticMaster	N/A
Loueriro et al., 09	Stroke	N/A	Arm and Hand	Reach and Grasp	Genlte/G, HapticMaster	FMA
Lum et al., 02	Stroke	N/A	Arm	Reaching	MIME	FMA, Barthel Index, FIM
Luo et al., 05	Stroke	N/A	Upper Limb	Grasp & Release	BPO, PPD	CAHAI
Merians et al., 02	Stroke	Left	Hand Functions	Range of Motion, Finger Fractionation, & Strength	CyberGlove, RMII-ND	Jebsen Test of Hand Function FMA
Mihelj et al., 08	Stroke, Healthy	N/A	Upper limb	Reach & Grasp	HenRiE, HapticMaster	N/A
O'Malley et al., 06	Stroke	N/A	Upper limb	Reach	RiceWrist	N/A
Nagaraj & Constantinescu, 09	Healthy	N/A	Upper limb	Pushing Cubes	Novint Falcon	N/A
Podobnik et al., 09	Hemiparetic Stroke	Left	Right limb	Pick & Place	HenRiE	N/A
Reiner et al., 04	Healthy	N/A	N/A	Ball & Block	PHANToM	N/A
Rozario et al., 09	Stroke	N/A	Upper Limb/ Attention, Vision	Path Following	PHANToM, WREX	FMA, WMFT, Box and Blocks Test, Functional Ability Scale
Shadmehr et al., 97	Healthy	N/A	Arm	Path Trajectories	Manipulandum	N/A
Stienen et al., 11	Stroke	N/A	Arm	Reaching	ACT 3D/ACT-4D	N/A
Takahashi et al., 05, 08	Chronic Stroke	N/A	Hand	Grasp & Release	HWARD	FMA, Box and Blocks Test, Action Research Arm Test
Viau et al., 04	Healthy, Unilateral Hemiparesis	Left	Right arm paresis	Grasp & Release	CyberGrasp	CAHAI
Volpe et al., 00	Stroke	N/A	Upper & lower limbs	Drawing Targets	MIT-Manus	FMA, Motor Power Score, Motor Power Status

To control errors, Rozario and colleagues (2009) used a PHANToM 3.0 and a WREX gravity-balanced rest to counterbalance the weight of each participants arm to potentially re-learn motor functions with a physical therapist. During the task, participants followed a cursor that the therapist controlled. The force feedback allowed them to correct their trajectories after an error has been made.

The Novint Falcon is commonly used for video gaming but has the potential to be used in rehabilitation research as a home based therapy. Chortis and colleagues (2008) asked stroke patients to use the Novint Falcon in their home by asking them to complete exercises that targeted pulling, pushing, reaching, and grasping. While, Nagaraj et al. (2009) used this device in a virtual environment to see how vibrations feedback changed muscular activity in the forearm and upper arm in order to develop an efficient program of rehabilitation.

Unlike the PHANToM and other end-effector devices, research involving the MIT-Manus has looked at kinesthetic information in a reaching task that targets the elbow and shoulders in regards to planar training (Krebs et al., 2004; & Finley et al., 2005). Krebs et al. (2004) conducted a study that looked at the effectiveness of this device when combined with planar training on rehabilitating arm movements in stroke patients. The MIT-Manus has also been used in exercises that involve an intense-short term rehabilitation technique that included a reaching task (Krebs et al., 2004; & Finley et al., 2005). Tasks that involved MIME have participants engaged in reaching exercises by themselves (active), feeling the feedback of the movement they produced (constrained), and initiating the movement with help of the device (passive) in a physical environment (Lum et al., 2002). Finally, devices that incorporate MIME, the MAHI and RiceWrist

have been used in the rehabilitation of movement in stroke and persons who suffer from spinal cord injury by asking them to perform reaching tasks, target hitting, and ADL tasks that involve eating and drinking (O'Malley et al., 2006; Pehlivan 2011; & Yozbatiran et al., 2012).

End-effector devices alone cannot be used to study grasping and fine finger movements; ungrounded exoskeleton devices are commonly used in conjunction to overcome this limitation. Tasks with ungrounded devices target most of the time human hand functioning such as grasping and finger movements. For instance, Subramanian et al. (2007) investigated how stroke patients completed a virtual elevator button pushing training with a 22 sensor CyberGlove. Since the glove does not provide haptic feedback, other sensory feedback (visual and auditory) was used to help hand and finger's orientation in the virtual environment (Subramanian et al., 2007). CyberGlove was also used in reaching and grasping tasks that involved moving and placing virtual objects to a new location (Finley et al., 2005). Similarly, HenRiE was used in a study that focused on activities of daily life that pertained to grasp and reach such as displacing a cup and placing it down onto a stand (Podobnik et al., 2009).

Combined with RMII, CyberGlove is also commonly used in virtual tasks that allow determining hand range of motion such as wiping off a window that reveals a landscape picture (Jack et al., 2001; & Boian et al., 2002), speed of movement such as catching a ball by measuring the speed of hand closing (Jack et al., 2001; & Merians et al., 2002), and finger fractionation (Jack et al., 2001; Merians et al., 2002; & Boian et al., 2002), Other research has used RMII for tasks that involved piston displacement with finger strength exercises (Boian et al., 2002; & Finley et al., 2005).

PURE-FORM has been used in tasks that involved objects and shapes orientation of objects (Frisoli et al., 2005; & Frisoli et al., 2011); while GRAB was used in tasks that involve pick and place (Bergamasco et al., 2006) and sphere catching while combined with ARMEO (Cameirao et al., 2012). Fine motor movement tasks have been investigated with HIRO-III in tasks that involved hand opening and finger pinching in a non-virtual environment (Endo et al., 2011; & Hioki et al., 2011). HWARD was used in real-life daily life tasks pertaining to the grasping and releasing of real or virtual objects that targeted range of motion, speed, and completion time of the task (Takahashi et al., 2005).

Extensive research with HapticMaster, when combined with other hand orthotics, has been used in tasks involving attention, motivation, reaching, catching, and grasping of virtual and real-life objects (Van der Linde, 2002; Loureiro et al., 2003; Loureiro et al., 2007; Loureiro et al., 2009; & Ziherl et al., 2010). In ADLER environment, functional hand movements' tasks were design to allow the patient manipulating 3D and real-life objects through grasping (Johnson et al., 2008; Wisneski & Johnson, 2008; Johnson et al., 2011). ACT-4D system allowed the affected limb to move horizontally while the HapticMaster moves the arm vertically in reaching tasks that involved shoulder-abduction and elbow stretching (Sukal et al., 2006; & Stienen et al., 2011). ARMin was also used in virtual ADL tasks that provide the user with visual, sensory, and auditory cues about the different objects and virtual environments (Nef et al., 2007; & Guidali et al., 2011).

To demonstrate the effectiveness of L-Exos and the potential use in a clinical rehabilitation setting, participants completed virtual reaching or target tasks. They also

took part in circular pursuit and object manipulation tasks where they were instructed to create an image that was in the background of the VE (Frisoli et al., 2008; Frisoli et al., 2009b; & Frisoli, 2009c). The BRAVO system, which uses L-Exos, was placed on the affected limb in conjunction with EMG on the non-affected limb in a grasping task. Throughout this task, participants were instructed to grip the object with the non-affected limb. The force produced by the non-affected limb would then be transferred through the EMG to the affected limb to generate a similar grasp (Lonconsole et al., 2013).

In summary, both grounded and ungrounded devices demonstrates a variety of different virtual scenarios that could promote ADLs that involve reaching and grasping objects, pursuit and trajectory tasks, and orientation tasks. While grounded exoskeleton can be used for fine motor movements of the finger; grounded robotic devices allow to adapt the task adaptability to the range of motion of the affected arm.

3.3. PARTICIPANTS' PERFORMANCES

Performance on the wide variety of tasks is based on the individual themselves and the type of motor assessments used to determine the therapy efficiency. Other factors related to the type of the device used, the VR program, and/or the task chose to improve motor functioning could also affect individuals' performances.

Stroke patients who had received training tasks that combined the Phantom with VR shown an increase in motor movements of their affected limb and in the scores obtained using the Box and Block and AMPS assessment methods (Broeren et al., 2004; & Broeren et al., 2007) suggesting the efficacy of VR haptic combination. Similarly, the PHANToM has been shown to also increase attention in TBI patients when presented with different haptic sensations through using the stylus in a virtual scenario scoring 75

on a GOAT assessment test. Sensations included being repelled or attracted to a target (Dvorkin et al., 2009), nudging or popping a balloon (Larson et al., 2011), judging haptically and visually the presence or the absence of an object (Reiner et al., 2004). Krebs et al. (2004) showed that after three weeks usage of the MIT-Manus, 250 stoke patients showed improvements in the impaired movements as a result of intense repetitive motions through the device, depicted by the scores of FMA, MS, MP, and Modified Ashworth scale. Other studies have showed similar FMA and WMFT score increases in 49 stroke patients using MIT-Manus over 12 and 36 week therapy comparing to patients who received usual care (Lo et al., 2010).

Using RMII, Jack et al. (2001) showed that after a two weeks training in a VR setting, thumb range of motion improved by 9-25% in three stroke patients, while their grasping force improved from 13% to 59% for one patient (Merians et al., 2002). Stroke patients completed tasks in a virtual environment with the RMII and CyberGlove during a three week period exhibited an increase in speed and strength of hand movements as indicated by the Jebson Test of Hand Function; while each of the participants decreased their average task completion times by 23-28% (Boian et al., 2002; & Adamovich et al., 2005).

Using CyberGlove and CyberGrasp, researchers (Viau et al., 2004) showed that both healthy and stroke participants had the tendency of decreasing their wrist extension and increasing their elbow extension. This could be due to the missing depth cues in a 2D environment that could be resolve using a head-mounted display (HMD). The type of haptic feedback needs also to be relevant to the task especially that the physical contact with the virtual object is missing in VR (Subramanian et al., 2007; & Viau et al., 2004).

PPD and BPO have also been shown to improve finger extension speed in stroke patients; also depicted by higher Box and Block and Rancho scores (Luo et al., 2005).

Podobnik et al. (2009) and (2011) indicated through one month training with HenRiE that two stroke patients improved strength opening and closing in grasping and reaching tasks. Podobnik et al. (2011) also indicated that when moving an object in a pick and place task, a healthy person could anticipate the grasp force to pick up the object; while stroke patients tend to use less grip force during the release phase; while the haptic path is not affected during the grasp phase, probably due to the small haptic feedback during the release phase.

Ungrounded devices have illustrated positive benefits with virtual reality in regaining motor movements in stroke individuals as depicted by a variety of motor assessments. However, the progress of each patient is pertained to the type of haptic device and tasks involved (Merians et al., 2002; Boian et al., 2002; & Loureiro et al., 2009) which can greatly impact the level of improvement of each person. Indeed, not all patients displayed progress; some showed improvements in some tasks while others did not. One plausible explanation is related to skill level used in the training; one person may be able to fully grasp an object while another would need assistance with the hand opening and closing. It has been recommend that when designing grasping and reaching tasks for stroke patients, the movement should be further broken down into several paths (Podobnik et al., 2011) such as, for instance, grasp, trajectory movement, and then release. This could help identify where stoke individuals have issues executing the movement which in turn could lead to the development of an environment that could be designed to the specific needs of that person. Similarly, to end-effector and ungrounded

devices, grounded robotics research indicates an increase in upper limb functioning as reported by clinical assessment scores (Stienen et al., 2011; & Lo et al., 2010) and research with healthy participants to establish a baseline for movement comparison (Johnson et al., 2008).

Studies with grounded robotic devices, such as L-Exos, have suggested that they can increase reaching motions while decreasing completion times. Indeed, patients decreased completion times by 50 to 70 % in three patients (Frisoli et al., 2008). Loureiro et al. (2001) demonstrated that robotic therapy coupled with virtual reality can provide an additional motivational factor to patients comparing to traditional therapy; confirmed by patients' feedback. Indeed, participants who completed their training with Gentle/G had shown a greater recovery in reaching movements than those who received physical therapy (Loureiro et al., 2009). Other studies have investigated the effects of robotic and haptic devices in real life tasks. Real life tasks take longer to complete for stroke patients comparing to healthy participants. Using ARMin, and virtual scenarios such as cooking and cleaning, stroke patients took four times longer to finish the task comparing to healthy individuals; the grasping phase being the longest. It can be challenging for stroke patients to coordinate the real movement to a virtual grasp of 3D virtual objects perceived on a 2D screen; even with assistance of ARMin, as participants stated that the VE seems unnatural (Guidali et al., 2011); an issue that could potentially be resolved by HMDs.

Lum et al. (2002) showed that stroke patients who received robotic therapy via MIME performed better than those who were in the physical therapy condition. ARMEO and GRAB showed positive outcomes for stroke patients as well. Indeed, in virtual environment training of a group of 44 stroke participants, the results showed an increase

in their abilities to complete ADLs successfully using three RGS: RGS, RGS-H (Haptic), and RGS-E (Exoskeleton), although none significant differences were found between the three systems suggesting that VR play a key role in patients' rehabilitation and the haptic feedback could be adapted to specific tasks to be fully exploitable. Patients who used RGS along with a traditional therapy displayed a better motor functioning improvement than the ones who went through physical therapy only as depicted by the pre and post FMA, CAHAI, and Barthel Index assessment scores (Cameriao et al., 2012).

Using PURE-FORM, Frisoli et al. (2011) compared the usage of kinesthetic feedback, cutaneous feedback, and combined kinesthetic-tactile feedback. Their results showed that better performances were obtained by combined modalities in discriminating objects orientation. The tactile feedback was not affected by the object size, while the kinesthetic feedback was affected by small sizes. However, one used alone, the cutaneous feedback condition required a longer completion time due to the missing kinesthetic feedback (Frisoli et al., 2011). The results suggest that PURE-FORM could be used on persons with upper limb paralysis to re-learn tactile information of objects.

A general trend can be observed when comparing performances of all of the devices. There is clear evidence that haptic feedback increase upper limb motor functioning. The best performances, and that could lead to better outcomes are, however, they ones that could be customizable to the individual's needs.

3.4. CONCLUSION

In this literature review, we presented the most commonly used haptic devices in neurorehabilitation and their impact on the rehabilitation of motor and cognitive problems seen in brain damaged individuals. Although these devices contribute in the

advance of the field of haptic neurorehabilitation, more research is needed to help restore a patient's full haptic sensations that include cutaneous, proprioceptive, and kinesthetic feedback. Full understandings of the different brain areas associated with various types of brain damage as well as with different haptic and tactile sensations are also necessary to better target the part of the paralyzed human body that has been affected by brain damage. It is also necessary to develop better methods that allow transferring activities completed in virtual environment (VE) to a real home or work environment.

Research must also take in account individual differences. Indeed, each person has various capabilities to perform a specific task and this fact transfers to a person suffering from a brain lesion or paralysis. Devices that work for some individuals might not work for others which can be discouraging for the person undergoing rehabilitation. A more individualized device or virtual task was suggested to solve this issue (Broeren et al., 2004; & Broeren et al., 2007).

Most of the research presented in this review has focused on the kinesthetic and proprioceptive senses. Since few devices include tactile and cutaneous sensations, which can be lost in combination with motor movement, it may be possible to increase these sensations through tactile vibrations or thermic sensations to help restore current (medial lemniscal pathway for touch sensations and spino-thalamic pathway for temperature) or new neural pathways that could to provide sufficient information about texture and temperature.

Another promising alternative rehabilitation technique for severely paralyzed or amputee persons is brain computer interface (Rossini et al., 2010). Brain computer interface is a way to communicate with the outside world by means of brain activity that

is recorded and processed in real time to reflect user's intent (for instance moving a robotic arm). Haptic or vibrotactile feedback could be very useful to close the loop in BCI. For instance, patients could think about the movement to perform, a mechanism known as mental imagery (Steffin, 1997). This intended brain activity is transmitted and captured by the BCI and then transduced into a command to control the robotic mechanism (Gomez-Rodriguez et al., 2010a; Gomez-Rodriguez et al., 2010b; Escolano et. al., 2010; & Christiansen et al., 2013). For instance, Christiansen et al. (2013) attached EMG electrodes and a vibrotactile device to participants arms to control a virtual prosthetic with brain activity. During the task, each participant received visual and tactile feedback. They found that vibrotactile feedback could be used as a means of informing the participant about the virtual prosthetic.

Finally, the development of haptic devices should also focus on interaction with physical and tangible objects. Humans interact with physical objects on a daily basis and having participants interact with real objects could improve the outcomes of successfully rehabilitating lost functions as a result of brain injury. It may be more beneficial for neurorehabilitation research to investigate how physical objects and virtual ones relate to improving neuronal connections in the brain. Thus, Frisoli et al. (2012) showed a promising technique that uses eye gaze and BCI as a means of interacting with physical objects by controlling a robotic arm with brain activity in stroke patients as well as healthy individuals. Kinect and an eye tracker were also used to assist objects' localization. Interestingly, there was no difference between stroke and healthy individuals' performances while locating objects. This study suggests that this new BCI

method, by incorporating multi-modal aspects of functioning, can be beneficial to stroke victims (Lonconsole et al., 2013).

In summary, different devices have been used to help individuals with upper limb deficiencies after a traumatic event to the brain or spinal cord. However, further research is still needed to determine how these devices could increase neuronal connections during neurorehabilitation (Reinkensmeyer, 2004; & Johnson, 2006). Research is also needed to investigate the best method for combining physical therapy with haptics and virtual reality, as several research demonstrated the benefits of using VR during a haptic therapy. VR itself has shown to be beneficial in rehabilitation of brain damaged patients (Rizzo et al., 2005; & Adamovich et al., 2009).

CHAPTER 2: A NIGHT LANDING TASK USING A HAPTIC FEEDBACK

1. INTRODUCTION

As mentioned in chapter one, several tasks were designed to target neurorehabilitation with haptic devices. These tasks allowed the interaction with simple objects such as balls and blocks. Participants were required to either display an object from one location to another or perform a pursuit task to a specific target. We opted for the latter by using a landing task. Indeed, piloting scenarios could potentially be interesting paradigms for neurorehabilitation research, as they require 3D spatial navigation and could increase motor movement capabilities of upper limbs paralysis after training.

2. THE BLACK HOLE ILLUSION

Landing an airplane requires great skill, training, and visual acuity. During high visibility conditions, pilots rely on what is known as out the window views of the environment which gives visual and salient cues pertaining to the speed, altitude, angle of distance, pitch, and environmental textures which allows for proper control of the airplane (Foyle, Kaiser, & Johnson, 1992; & Bulkley, Dyre, Lew, & Caufield, 2009). To compensate for the lack of physical features during night landing, runway edge lights are used to provide information about runway boundaries (Gibb, 2007). However, when trying to land an airplane in a featureless night such as no stars or moonlight, pilots might overestimate the glide path caused by what is known as the black hole illusion (BHI)

(Mertens & Lewis, 1981; Holmes et al., 2007; Gibb, 2007; & Nicholson & Stewart, 2013). This manoeuver is called the glide path overestimation (GPO) that leads to inappropriate steep or tilted descent (See Figure 20). Since pilots often rely on visual sense during night landing rather than cockpit instruments (Thompson, 2009), adding a tactile feedback to give information about directional clues could help them redress the aircraft to line-up with the horizon.

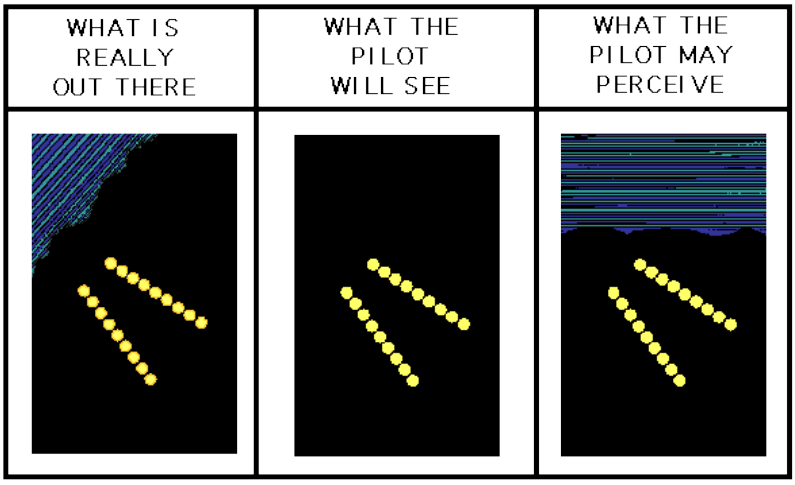

FIGURE 20. LEFT) THE HORIZON LINE IN THE ACTUAL ENVIRONMENT, CENTER) THE ENVIRONMENT AS SEEN BY THE PILOT DOES NOT CONTAIN AS VISUAL CUES, EXCEPT FOR THE RUNWAY LIGHTS, RIGHT) THE BLACK HOLE ILLUSION: THE HORIZON LINE CAN BE MISPERCEIVED (FROM WATSON, 1992).

Indeed tactile vibrations have been successfully introduced by The United States Army that developed the Tactile Situation Awareness System (TSAS), a vest that provides vibrotactile stimulation to the trunk of the body informing the pilot about altitude, location, and navigational information (Chiasson, McGrath, & Rupert, 2003; & McGrath et al., 2004). van Erp et al. (2006) used a similar vest that provided tactile feedback to the torso during a flight simulation task and reported that tactile stimulation

could help prevent spatial disorientation which is commonly experienced in the black hole illusion.

As an alternative to tactile vests, it is possible to provide tactile information to the pilot on the control column (wheel) regarding the environment. In our original approach, we planned to provide tactile feedback on the hand, and more specifically the fingertips, to investigate whether minimal tactile directional information could help the person redresses her trajectory. For technical reasons, the tactile feedback was not operational on time for the scope of this thesis. Therefore, we decided to explore whether a force feedback could affect the trajectory of the landing.

3. EXPERIMENT

In this experiment, we developed a virtual landing task to evaluate participants' performances with and without haptic feedback. The scenario is similar to the BHI, except that runway edge lights were removed in order to simplify the virtual scenario. We also used a featured night landing that provided information on the horizon as a control condition comparing to the featureless night landing situation. Expect for the distal direction (forward) where participants moved at a predetermined speed, we expected haptic feedback to enhance glide path accuracy for the mediolateral (left-right) and superioproximal (up-down) during night condition compared to a night conditions that does not provide any visual or haptic information. We also expected haptic feedback to improve the trajectory during the featured night condition; although we anticipated any difference to be smaller in relation to the featureless condition.

3.1. PARTICIPANTS

Sixteen (9 females and 7 males) aged between 18 and 43 (mean = 24, SD = 7.97) took part in this experiment. They were PY100 (introduction to psychology) students from Northern Michigan University participated in this experiment and received course credit for their participation. None of them had any previous experience with a haptic device or flying an aircraft. Participants gave their informed consent before participating and the procedures were approved by the Institutional Review Board at Northern Michigan University.

3.2. APPARATUS AND STIMULI

For this experiment, we used a haptic device known as the PHANToM OMNI (Geomagic) described previously in chapter (3.1). The PHANToM OMNI is a 6 DOF device that provides force feedback about objects in the virtual environment. The virtual environment was developed using H3D API, an open source software with OpenGL standards, to create haptic and graphic representations within the virtual world (Appendix A and Appendix B). Figure 21 shows stimuli which consisted of a virtual runway in four different conditions: (1) featured night with haptic feedback (FH), (2) featured night without haptic feedback (FWH), (3) featureless (non-featured) night with haptic feedback (NFH), and (4) featureless night without haptic feedback (NFWH). The haptic feedback gets stronger when participants deviates from the center (they would feel a force pushing them back toward the center), inciting them to return back to the center.

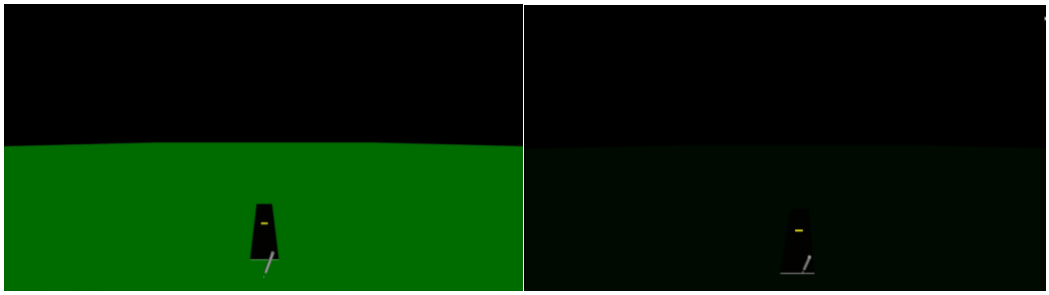

FIGURE 21. VIRTUAL RUNWAYS FOR FEATURED NIGHT (LEFT) AND FEATURELESS NIGHT (RIGHT) CONDITIONS.

3.3. PROCEDURE

After reading instructions (See Appendix C) and informed consent (See Appendix D), participants were seated comfortably in a chair in front of a computer monitor. Next, they were instructed to and place their dominant hand on the stylus to complete a training task; all the participants were right handed. The training task consisted of interacting with a tower of blocks that could be moved by holding the stylus of the haptic device. The contact with each block provided a force feedback (resistance) that participants could feel and which informed them that they are in contact with the virtual object. The training phase, which lasted about 5 minutes, allowed participants to become familiarized with the haptic device in order to understand its interaction with the virtual objects and movement within a 3-dimensional space. Next, participants were asked to complete two practice trials of the actual experiment to become acquainted with the virtual environment.

After the training session, participants were instructed to land the flying cursor (a virtual stylus) on a specific landmark (yellow rectangle) on the runway. The trial ended when they reached the landmark. The virtual runway was used to assess participants' accuracy of landing a virtual object under the four conditions previously mentioned and

presented randomly using an ABC-CBA scheme to avoid order effect. Each participant completed a total of 16 counterbalanced trials (each condition presented four times). There were no time constrains and the completion time was recorded for each trial. Performance was measured by the position of the stylus (the 3 Cartesian coordinates) and the time to complete each trial. We expected the haptic condition to improve landing accuracy in the featured and featureless night conditions.

3.4. Data Analysis

The 3D trajectory movements produced by the haptic device resulted in a large data set of Cartesian coordinates. We opted for a principle components analysis (PCA), a powerful statistical method used for continuous variables. In our case it was be used to determine the correlation between the different conditions: NFH, NFWH, FH, and FWH between participants for the 3 Cartesian coordinates. The PCA occurred in two steps: 1) data reduction that consisted of extracting the factors for further analysis; 2) predicted the relationship between components extracted in phase one. We also recorded the completion time of each trial and analyzed with a repeated measures ANOVA.

3.5. Results

3.5.1. Participants' trajectory for x, y, and z for each condition

This section presents the results for each axis for each condition for all the participants. The x-axis is the movement along the mediolateral direction (anatomical coordinates) that represents the left-right direction. The y-axis is the movement along the superior-proximal direction that represents the up-down trajectory (towards and away

from the head). Finally, the z-axis is the hand movement along the distal direction, which is the direction away from the trunk (anterior direction).

a. Featured night with haptic

Figure 22 shows the scree plots that allowed us to extract the components for the PCA analysis. The square shows the inflexion point that indicates where the slope changed drastically. The number of components extracted is to the left of the inflexion point. For instance, Figure 22a shows the inflexion point at 4, which means the number of extracted components is 3.

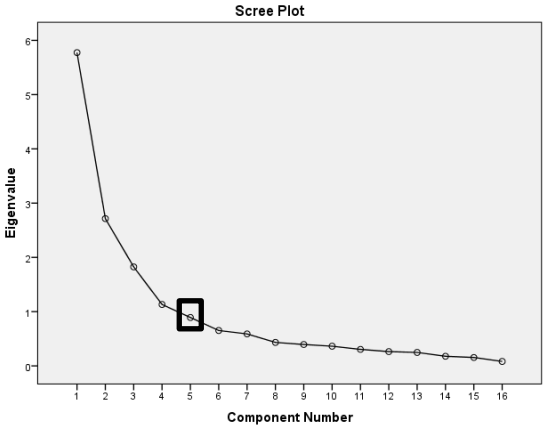

A

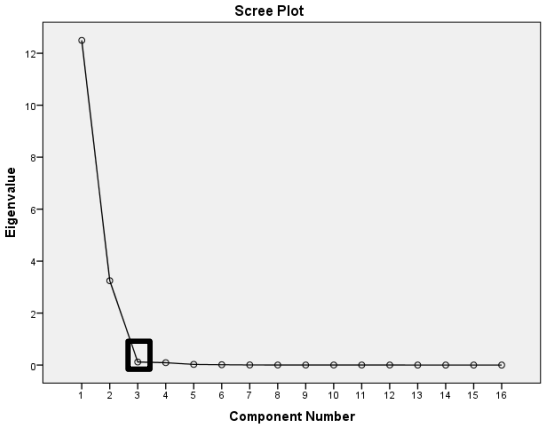

b

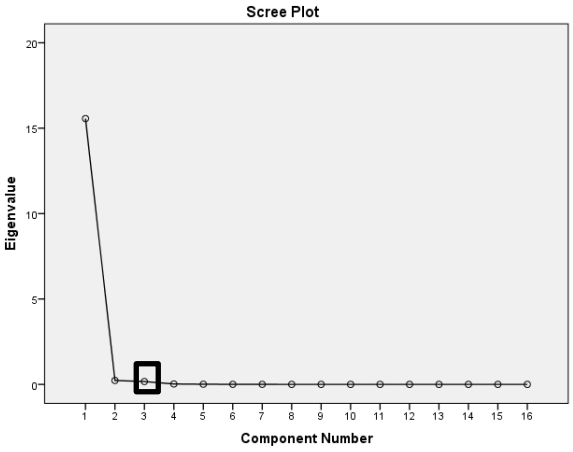

c

FIGURE 22. SCREE PLOTS SHOWING THE INFLECTION POINT (SHOWN BY THE SQUARE) FOR A) X, B) Y, AND C) Z DIRECTIONS FOR THE FH CONDITION.

For the mediolateral direction (left-right), a PCA was conducted on 16 participants with oblique rotation (promax). The Kaiser-Meyer-Olkin measure verified the sampling adequacy for the analysis, KMO= .78 ('good' according to Field, 2009), and as shown by Table 3, all KMO values for individual participants were > .618, which is well above the acceptable limit of 0.5 (Field, 2009). Bartlett's test of sphericity χ^2 (120) = 27424.55, $p < .001$, indicated that correlations between participant's performances were sufficiently large for PCA. An initial analysis was run to obtain eigenvalues for each component in the data. Three components had eigenvalues over Kaiser's criterion of 1 and in combination explained 64.46% of the variance. The scree plot (see Figure 22a) showed inflexions that would justify retaining three components in the final analysis.

TABLE 3. KMO VALUES FOR ALL PARTICIPANTS FOR THE X-AXIS (FH CONDITION). VALUES FOR INDIVIDUAL PARTICIPANTS ARE HIGHLIGHTED IN GREY (SIGNIFICANT > 0.5).

Anti-image Matrices

		P1	P2	P3	P4	P5	P6	P7	P8	P9	P10	P11	P12	P13	P14	P15	P16
Anti-image Correlation	P1	.629a	.239	.102	.062	-.299	.163	.025	-.344	-.029	.191	-.138	-.134	.182	-.113	.124	-.002
	P2	.239	.747a	.224	-.261	-.469	-.303	.037	-.583	.113	-.227	-.187	-.025	.030	.167	.419	.215
	P3	.102	.224	.827a	-.192	-.125	-.366	-.096	-.238	.194	-.068	-.291	-.118	-.003	.148	.115	.132
	P4	.062	-.261	-.192	.911a	.047	-.082	-.138	-.083	-.225	-.058	.103	-.018	-.067	-.055	-.240	.017
	P5	-.299	-.469	-.125	.047	.655a	.113	-.132	.234	-.167	.310	.050	.104	-.082	-.025	-.174	-.227
	P6	.163	-.303	-.366	-.082	.113	.887a	.041	.057	-.027	-.011	-.036	.014	.117	-.116	.023	.173
	P7	.025	.037	-.096	-.138	-.132	.041	.870a	-.329	-.003	-.221	-.367	-.225	.105	-.143	-.083	.235
	P8	-.344	-.583	-.238	-.083	.234	.057	-.329	.776a	-.127	.161	.265	.075	.027	-.260	-.187	-.155
	P9	-.029	.113	.194	-.225	-.167	-.027	-.003	-.127	.723a	-.033	.051	-.149	.099	-.141	.229	.074
	P10	.191	-.227	-.068	-.058	.310	-.011	-.221	.161	-.033	.663a	.245	.167	.070	-.300	-.238	-.218
	P11	-.138	-.187	-.291	.103	.050	-.036	-.367	.265	.051	.245	.796a	.393	-.187	-.254	.131	-.039
	P12	-.134	-.025	-.118	-.018	.104	.014	-.225	.075	-.149	.167	.393	.695a	.100	.223	.305	-.229
	P13	.182	.030	-.003	-.067	-.082	.117	.105	.027	.099	.070	-.187	.100	.812a	-.425	.194	-.083
	P14	-.113	.167	.148	-.055	-.025	-.116	-.143	-.260	-.141	-.300	-.254	.223	-.425	.804a	.157	-.263
	P15	.124	.419	.115	-.240	-.174	.023	-.083	-.187	.229	-.238	.131	.305	.194	.157	.618a	.177
	P16	-.002	.215	.132	.017	-.227	.173	.235	-.155	.074	-.218	-.039	-.229	-.083	-.263	.177	.677a

a. Measures of Sampling Adequacy(MSA)

For the superior-inferior direction (up-down), an initial analysis was run to obtain eigenvalues for each component in the data. Two components had eigenvalues over Kaiser's criterion of 1 and in combination explained 98.38% of the variance. The scree plot (Figure 22b) showed inflexions that would justify retaining two components in the final analysis. The Kaiser-Meyer-Olkin measure verified the sampling adequacy for the analysis, KMO= .87 ('good' according to Field, 2009), and as shown by Table 4, all KMO values for individual participants were superior .80, which is well above the acceptable limit of 0.5 (Field, 2009). Bartlett's test of sphericity χ^2 (120) = 182262.68, $p < .001$, indicated that correlations between participant's performances were sufficiently large for PCA.

TABLE 4. KMO VALUES FOR ALL PARTICIPANTS FOR THE Y-AXIS (FH CONDITION). VALUES FOR INDIVIDUAL PARTICIPANTS ARE HIGHLIGHTED IN GREY (SIGNIFICANT > 0.5).

Anti-image Matrices

		P1	P2	P3	P4	P5	P6	P7	P8	P9	P10	P11	P12	P13	P14	P15	P16
Anti-image Correlation	P1	.822[a]	-.293	-.341	-.097	-.081	-.273	.322	.281	.482	.048	-.068	-.234	.081	-.020	-.135	.068
	P2	-.293	.931[a]	.026	.133	-.159	-.124	-.656	-.026	-.080	.048	.340	-.143	.246	.061	-.094	.125
	P3	-.341	.026	.712[a]	-.298	.202	-.116	-.155	.234	.277	-.497	.276	.164	.242	.535	-.576	-.140
	P4	-.097	.133	-.298	.898[a]	-.371	-.344	-.085	-.355	-.423	.234	.037	.174	-.234	.031	.111	-.087
	P5	-.081	-.159	.202	-.371	.956[a]	-.264	.233	.122	.126	-.131	-.036	-.002	-.307	-.173	.068	.057
	P6	-.273	-.124	-.116	-.344	-.264	.862[a]	-.186	-.554	-.355	.028	-.175	.195	-.095	-.174	.496	-.045
	P7	.322	-.656	-.155	-.085	.233	-.186	.929[a]	.028	.152	.100	-.087	.032	-.372	-.142	-.007	-.122
	P8	.281	-.026	.234	-.355	.122	-.554	.028	.851[a]	.614	-.158	-.090	-.415	.588	.210	-.614	.192
	P9	.482	-.080	.277	-.423	.126	-.355	.152	.614	.865[a]	-.173	-.137	-.324	.538	-.094	-.438	.164
	P10	.048	.048	-.497	.234	-.131	.028	.100	-.158	-.173	.892[a]	-.244	-.611	.025	-.440	.218	.480
	P11	-.068	.340	.276	.037	-.036	-.175	-.087	-.090	-.137	-.244	.930[a]	.207	-.310	.369	-.114	-.490
	P12	-.234	-.143	.164	.174	-.002	.195	.032	-.415	-.324	-.611	.207	.846[a]	-.592	.168	.167	-.843
	P13	.081	.246	.242	-.234	-.307	-.095	-.372	.588	.538	.025	-.310	-.592	.803[a]	.087	-.502	.623
	P14	-.020	.061	.535	.031	-.173	-.174	-.142	.210	-.094	-.440	.369	.168	.087	.885[a]	-.710	-.177
	P15	-.135	-.094	-.576	.111	.068	.496	-.007	-.614	-.438	.218	-.114	.167	-.502	-.710	.836[a]	-.108
	P16	.068	.125	-.140	-.087	.057	-.045	-.122	.192	.164	.480	-.490	-.843	.623	-.177	-.108	.865[a]

a. Measures of Sampling Adequacy(MSA)

For the z-axis (anterior direction), a PCA was conducted on 15 participants with oblique rotation (promax). One participant has been removed from the analysis for improperly recorded data. The Kaiser-Meyer-Olkin measure verified the sampling

adequacy for the analysis, KMO= .90 ('great' according to Field, 2009), and as shown by Table 5, all KMO values for individual participants were > .833, which is well above the acceptable limit of 0.5 (Field, 2009). Bartlett's test of sphericity χ^2 (120) = 274759.34, p < .001, indicated that correlations between participant's performances were sufficiently large for PCA. An initial analysis was run to obtain eigenvalues for each component in the data. One component had eigenvalues over Kaiser's criterion of 1 and in combination explained 97.27% of the variance. The scree plot (see Figure 22c) showed inflexions that would justify retaining one component in the final analysis.

TABLE 5. KMO VALUES FOR ALL PARTICIPANTS FOR THE Z-AXIS (FH CONDITION). VALUES FOR INDIVIDUAL PARTICIPANTS ARE HIGHLIGHTED IN GREY (SIGNIFICANT > 0.5).

Anti-image Matrices

		P1	P2	P3	P4	P5	P6	P7	P8	P9	P10	P11	P12	P13	P14	P15	P16
Anti-image Correlation	P1	.928[a]	.087	-.054	.015	.089	-.811	-.289	.339	.135	.010	-.382	-.216	.144	-.027	.082	-.105
	P2	.087	.885[a]	-.794	.268	-.477	-.168	.234	-.271	-.207	.079	-.589	.183	-.205	.161	.378	.080
	P3	-.054	-.794	.928[a]	-.254	.217	.151	-.026	.310	.047	-.293	.206	.027	-.008	-.263	-.219	-.108
	P4	.015	.268	-.254	.941[a]	.023	.207	-.044	-.442	.004	.090	-.050	-.099	-.036	-.039	.001	-.713
	P5	.089	-.477	.217	.023	.833[a]	-.026	-.645	.117	.514	.242	.291	-.857	-.190	-.585	-.817	-.119
	P6	-.811	-.168	.151	.207	-.026	.927[a]	.184	-.131	-.075	-.003	.286	.158	-.143	-.005	-.125	-.436
	P7	-.289	.234	-.026	-.044	-.645	.184	.857[a]	-.491	-.547	-.772	-.222	.490	-.052	.087	.358	.207
	P8	.339	-.271	.310	-.442	.117	-.131	-.491	.934[a]	.282	.334	-.238	-.013	-.033	.106	-.066	-.109
	P9	.135	-.207	.047	.004	.514	-.075	-.547	.282	.889[a]	.384	.036	-.587	-.387	-.491	-.450	-.118
	P10	.010	.079	-.293	.090	.242	-.003	-.772	.334	.384	.919[a]	.268	-.182	-.033	.339	-.124	-.124
	P11	-.382	-.589	.206	-.050	.291	.286	-.222	-.238	.036	.268	.930[a]	.028	.393	.196	-.053	.047
	P12	-.216	.183	.027	-.099	-.857	.158	.490	-.013	-.587	-.182	.028	.835[a]	.368	.648	.864	.084
	P13	.144	-.205	-.008	-.036	-.190	-.143	-.052	-.033	-.387	-.033	.393	.368	.912[a]	.560	.544	.030
	P14	-.027	.161	-.263	-.039	-.585	-.005	.087	.106	-.491	.339	.196	.648	.560	.877[a]	.643	.041
	P15	.082	.378	-.219	.001	-.817	-.125	.358	-.066	-.450	-.124	-.053	.864	.544	.643	.841[a]	.081
	P16	-.105	.080	-.108	-.713	-.119	-.436	.207	-.109	-.118	-.124	.047	.084	.030	.041	.081	.945[a]

a. Measures of Sampling Adequacy(MSA)

b. Featured night without haptics

The scree plots on Figure 23 shows the point of inflexion for X, and Y that allowed to extract the components for the PCA. Because of the highly correlated values for the z-axis, we only performed Pearson correlation, because the matrix was not positive definite (caused by the singularity of the data).

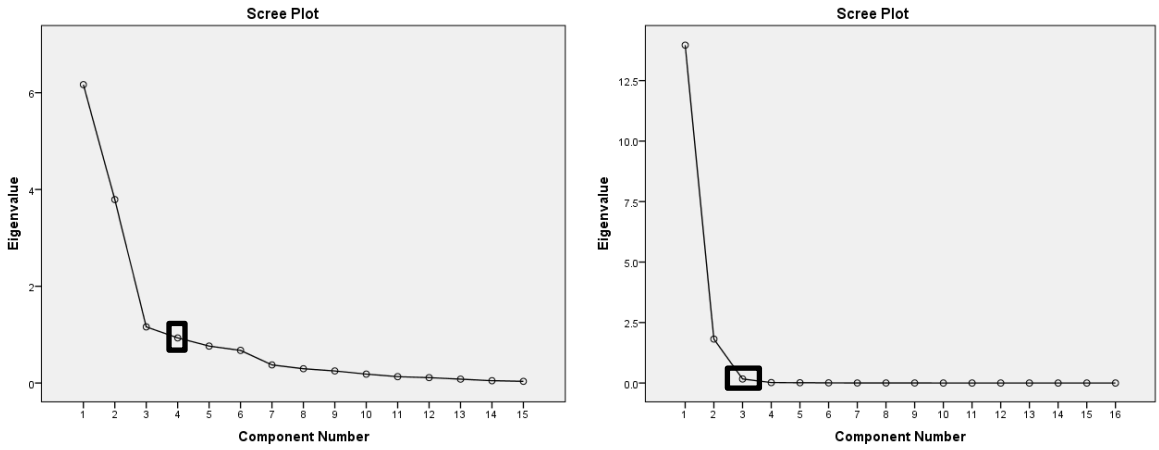

a b

FIGURE 23. SCREE PLOTS SHOWING THE INFLECTION POINT (SHOWN BY THE SQUARE) FOR A) X, AND B) Y DIRECTIONS FOR THE FWH CONDITION.

For left-right direction, a PCA was performed on the 15 participants with oblique rotation (promax). One participant was not included in this analysis due to an irregular landing trajectory. The Kaiser-Meyer-Olkin measure verified the sampling adequacy for the analysis, KMO= .739 ('good' according to Field, 2009), and as shown by Table 6, all KMO values for individual participants were > .562, which is well above the acceptable limit of 0.5 (Field, 2009). Bartlett's test of sphericity χ^2 (120) = 38737.63, $p < .001$, indicated that correlations between participant's performances were sufficiently large for PCA. An initial analysis was run to obtain eigenvalues for each component in the data. Three components had eigenvalues over Kaiser's criterion of 1 and in combination explained 74.13% of the variance. The scree plot (see Figure 23) showed that three components have been retained in the final analysis.

TABLE 6. KMO VALUES FOR ALL PARTICIPANTS FOR THE X-AXIS (FWH CONDITION). VALUES FOR INDIVIDUAL PARTICIPANTS ARE HIGHLIGHTED IN GREY (SIGNIFICANT > 0.5).

Anti-image Matrices

		P1	P2	P3	P4	P5	P6	P8	P9	P10	P11	P12	P13	P14	P15	P16
Anti-image Correlation	P1	.599[a]	.038	.401	.052	.263	.116	.045	.159	.038	.126	.012	.144	-.215	-.346	.096
	P2	.038	.562[a]	.248	-.003	.238	-.106	.194	-.090	-.191	.069	.028	.124	-.344	.097	.282
	P3	.401	.248	.625[a]	-.438	.555	-.035	.317	.130	.266	.314	.069	.222	-.365	-.186	.144
	P4	.052	-.003	-.438	.808[a]	-.180	-.372	-.292	.024	-.317	-.301	.021	-.252	.383	-.291	-.234
	P5	.263	.238	.555	-.180	.670[a]	-.100	.341	.233	-.086	.415	-.154	-.311	-.314	-.202	-.179
	P6	.116	-.106	-.035	-.372	-.100	.828[a]	-.341	-.305	.332	-.057	-.094	.333	-.270	-.148	.196
	P8	.045	.194	.317	-.292	.341	-.341	.775[a]	.096	-.474	.491	.192	-.286	-.267	.043	-.125
	P9	.159	-.090	.130	.024	.233	-.305	.096	.806[a]	-.199	.278	.421	-.364	-.228	-.075	.017
	P10	.038	-.191	.266	-.317	-.086	.332	-.474	-.199	.736[a]	-.477	-.299	.466	.217	-.162	-.019
	P11	.126	.069	.314	-.301	.415	-.057	.491	.278	-.477	.720[a]	.208	-.366	-.557	.068	-.152
	P12	.012	.028	.069	.021	-.154	-.094	.192	.421	-.299	.208	.702[a]	.034	-.550	.397	.186
	P13	.144	.124	.222	-.252	-.311	.333	-.286	-.364	.466	-.366	.034	.678[a]	-.157	.088	.372
	P14	-.215	-.344	-.365	.383	-.314	-.270	-.267	-.228	.217	-.557	-.550	-.157	.667[a]	-.286	-.389
	P15	-.346	.097	-.186	-.291	-.202	-.148	.043	-.075	-.162	.068	.397	.088	-.286	.828[a]	.258
	P16	.096	.282	.144	-.234	-.179	.196	-.125	.017	-.019	-.152	.186	.372	-.389	.258	.810[a]

a. Measures of Sampling Adequacy(MSA)

For the y-axis, a PCA was performed on the 16 participants with oblique rotation (promax). The Kaiser-Meyer-Olkin measure verified the sampling adequacy for the analysis, KMO= .88 ('great' according to Field, 2009), and as shown by Table 7, all KMO values for individual participants were > .701, which is well above the acceptable limit of 0.5 (Field, 2009). Bartlett's test of sphericity χ^2 (120) =214414.12, $p < .001$, indicated that correlations between participant's performances were sufficiently large for PCA. An initial analysis was run to obtain eigenvalues for each component in the data. Two components had eigenvalues over Kaiser's criterion of 1 and in combination explained 87.30% of the variance. The scree plot (see Figure 23) showed inflexions that would justify retaining two components that were retained in the final analysis.

Table 7. KMO values for all participants for the y-axis (FWH condition). Values for individual participants are highlighted in grey (significant > 0.5).

Anti-image Matrices

		P1	P2	P3	P4	P5	P6	P7	P8	P9	P10	P11	P12	P13	P14	P15	P16
Anti-image Correlation	P1	.701a	.265	-.381	.116	.181	-.386	-.731	-.095	.387	-.231	.528	-.135	-.382	.497	.037	-.173
	P2	.265	.908a	-.406	-.214	.550	-.300	-.436	-.468	.018	-.077	.037	-.338	-.132	.230	.084	.018
	P3	-.381	-.406	.808a	.049	-.435	.477	.404	-.054	-.509	-.134	.037	.721	.290	.253	-.241	.063
	P4	.116	-.214	.049	.921a	-.187	-.397	-.261	.019	.251	-.082	-.235	-.049	-.241	-.068	-.438	.572
	P5	.181	.550	-.435	-.187	.910a	-.407	-.290	-.415	.092	-.157	-.080	-.201	.099	-.002	.296	-.196
	P6	-.386	-.300	.477	-.397	-.407	.883a	.378	-.357	-.236	.128	.191	.266	.094	-.179	.230	-.236
	P7	-.731	-.436	.404	-.261	-.290	.378	.826a	.193	-.677	.302	-.476	.491	.539	-.352	-.169	.151
	P8	-.095	-.468	-.054	.019	-.415	-.357	.193	.953a	.034	.080	-.132	-.020	.133	.026	-.143	-.025
	P9	.387	.018	-.509	.251	.092	-.236	-.677	.034	.833a	-.102	.441	-.808	-.778	.033	.217	-.117
	P10	-.231	-.077	-.134	-.082	-.157	.128	.302	.080	-.102	.960a	-.121	-.180	-.050	-.208	-.379	.208
	P11	.528	.037	.037	-.235	-.080	.191	-.476	-.132	.441	-.121	.884a	-.185	-.620	.340	.215	-.393
	P12	-.135	-.338	.721	-.049	-.201	.266	.491	-.020	-.808	-.180	-.185	.848a	.615	.135	-.274	.109
	P13	-.382	-.132	.290	-.241	.099	.094	.539	.133	-.778	-.050	-.620	.615	.851a	-.135	.170	-.227
	P14	.497	.230	.253	-.068	-.002	-.179	-.352	.026	.033	-.208	.340	.135	-.135	.938a	-.185	-.154
	P15	.037	.084	-.241	-.438	.296	.230	-.169	-.143	.217	-.379	.215	-.274	.170	-.185	.885a	-.867
	P16	-.173	.018	.063	.572	-.196	-.236	.151	-.025	-.117	.208	-.393	.109	-.227	-.154	-.867	.888a

a. Measures of Sampling Adequacy(MSA)

For the z-axis, we originally performed a PCA. However, due to the highly correlated value, the PCA was unable to produce positive definite matrix. Pearson's r correlation was performed and the results showed significant correlations for the z-axis trajectory between all the participants (all the values are displaced in Table 8.

TABLE 8. PEARSON CORRELATION VALUES; SIGNIFICANT EFFECTS ARE SHOWN BY ASTERISKS.

	P1	P2	P3	P4	P5	P6	P7	P8	P9	P10	P11	P12	P13	P14	P15	P16
P1	1	.698**	.999**	.994**	.999**	.999**	.990**	.999**	.861**	.999**	.929**	.997**	.859**	.962**	.987**	.994**
P2	.698**	1	.705**	.759**	.701**	.692**	.746**	.702**	.243**	.692**	.863**	.733**	.962**	.857**	.587**	.638**
P3	.999**	.705**	1	.995**	1.000**	.999**	.993**	1.000**	.856**	.999**	.934**	.998**	.865**	.965**	.986**	.993**
P4	.994**	.759**	.995**	1	.995**	.995**	.992**	.995**	.815**	.995**	.949**	.997**	.900**	.985**	.970**	.983**
P5	.999**	.701**	1.000**	.995**	1	1.000**	.992**	1.000**	.860**	1.000**	.933**	.998**	.862**	.964**	.987**	.994**
P6	.999**	.692**	.999**	.995**	1.000**	1	.992**	1.000**	.866**	1.000**	.926**	.997**	.855**	.962**	.989**	.995**
P7	.990**	.746**	.993**	.992**	.992**	.992**	1	.993**	.812**	.992**	.935**	.993**	.888**	.973**	.965**	.975**
P8	.999**	.702**	1.000**	.995**	1.000**	1.000**	.993**	1	.858**	1.000**	.933**	.998**	.863**	.964**	.987**	.994**
P9	.861**	.243**	.856**	.815**	.860**	.866**	.812**	.858**	1	.866**	.656**	.835**	.489**	.704**	.926**	.899**
P10	.999**	.692**	.999**	.995**	1.000**	1.000**	.992**	1.000**	.866**	1	.926**	.997**	.855**	.962**	.989**	.995**
P11	.929**	.863**	.934**	.949**	.933**	.926**	.935**	.933**	.656**	.926**	1	.950**	.964**	.968**	.888**	.909**
P12	.997**	.733**	.998**	.997**	.998**	.997**	.993**	.998**	.835**	.997**	.950**	1	.886**	.974**	.980**	.989**
P13	.859**	.962**	.865**	.900**	.862**	.855**	.888**	.863**	.489**	.855**	.964**	.886**	1	.958**	.781**	.818**
P14	.962**	.857**	.965**	.985**	.964**	.962**	.973**	.964**	.704**	.962**	.968**	.974**	.958**	1	.915**	.938**
P15	.987**	.587**	.986**	.970**	.987**	.989**	.965**	.987**	.926**	.989**	.888**	.980**	.781**	.915**	1	.997**
P16	.994**	.638**	.993**	.983**	.994**	.995**	.975**	.994**	.899**	.995**	.909**	.989**	.818**	.938**	.997**	1

c. Featureless night with haptics

For the PCA analysis, Figure 24 shows the scree plots that were used to extract the components. These points, where the slope changed considerably, are indicated by the squares on each plot.

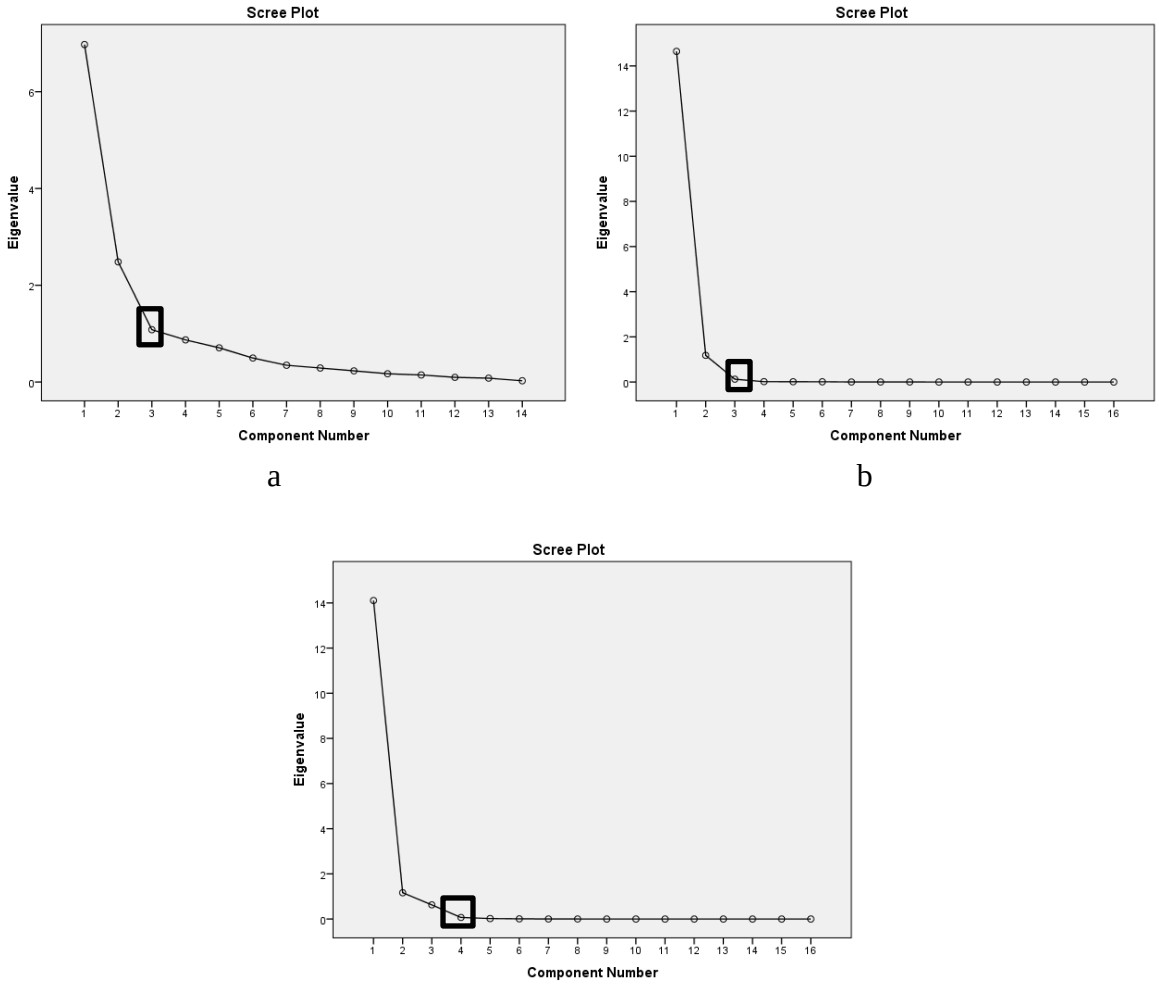

FIGURE 24. SCREE PLOTS SHOWING THE INFLECTION POINT (SHOWN BY THE SQUARE) FOR A) X, B) Y, AND C) Z DIRECTIONS FOR THE NFH CONDITION.

A PCA was conducted on 14 participants with oblique rotation (promax) for the mediolateral direction. Two participants' data were removed from the analysis for being

untrusted. An initial analysis was run to obtain eigenvalues for each component in the data. Two components had eigenvalues over Kaiser's criterion of 1 and in combination explained 67.56% of the variance. Kaiser-Meyer-Olkin measure verified the sampling adequacy for the analysis, KMO = .72 ('good' according to Field, 2009), and as shown by Table 9, all KMO values for individual participants were > .524, which is well above the acceptable limit of 0.5 (Field, 2009). Bartlett's test of sphericity χ^2 (120) = 22565.13, $p < .001$, shows that correlations between participant's performances were adequately large for PCA.

TABLE 9. KMO VALUES FOR ALL PARTICIPANTS FOR THE X-AXIS (NFH CONDITION). VALUES FOR INDIVIDUAL PARTICIPANTS ARE HIGHLIGHTED IN GREY (SIGNIFICANT > 0.5).

Anti-image Matrices

		P1	P3	P4	P5	P6	P8	P9	P10	P11	P12	P13	P14	P15	P16
Anti-image Correlation	P1	.831[a]	.294	-.065	-.091	.284	.098	-.171	.009	-.152	.077	-.072	-.162	-.193	-.031
	P3	.294	.603[a]	.273	-.466	-.460	.433	.066	-.388	-.531	-.303	.186	.126	.249	-.010
	P4	-.065	.273	.754[a]	-.469	-.357	.284	.199	-.361	-.581	-.108	-.028	.408	.276	.210
	P5	-.091	-.466	-.469	.623[a]	.295	-.632	.232	.749	.760	.138	-.035	-.374	-.310	.010
	P6	.284	-.460	-.357	.295	.811[a]	-.387	-.059	.283	.345	.201	-.045	-.116	-.085	.197
	P8	.098	.433	.284	-.632	-.387	.775[a]	-.014	-.296	-.577	-.098	-.107	.184	.130	.177
	P9	-.171	.066	.199	.232	-.059	-.014	.912[a]	-.087	.156	-.239	.194	.004	.349	-.148
	P10	.009	-.388	-.361	.749	.283	-.296	-.087	.654[a]	.520	.098	-.195	-.046	-.375	.350
	P11	-.152	-.531	-.581	.760	.345	-.577	.156	.520	.524[a]	.114	.109	-.535	-.125	-.163
	P12	.077	-.303	-.108	.138	.201	-.098	-.239	.098	.114	.688[a]	-.486	-.307	-.604	-.327
	P13	-.072	.186	-.028	-.035	-.045	-.107	.194	-.195	.109	-.486	.568[a]	-.304	.519	-.228
	P14	-.162	.126	.408	-.374	-.116	.184	.004	-.046	-.535	-.307	-.304	.755[a]	.260	.482
	P15	-.193	.249	.276	-.310	-.085	.130	.349	-.375	-.125	-.604	.519	.260	.687[a]	-.033
	P16	-.031	-.010	.210	.010	.197	.177	-.148	.350	-.163	-.327	-.228	.482	-.033	.849[a]

a. Measures of Sampling Adequacy(MSA)

PCA was performed on the 16 participants with oblique rotation (promax) for the y-axis direction. An initial analysis was run to obtain eigenvalues for each component in the data. Two components had eigenvalues over Kaiser's criterion of 1 and in combination explained 98.90% of the variance. The scree plot (see Figure 24) showed inflexions that will justify retaining two components in the final analysis. Table 10 shows the Kaiser-Meyer-Olkin measure verified the sampling adequacy for the analysis, KMO=

.85 (‘great’ according to Field, 2009), and as shown by Table XX, all KMO values for individual participants were > .689, which is well above the acceptable limit of 0.5 (Field, 2009). Bartlett’s test of sphericity χ^2 (120) = 151475.00, p < .001, indicated that correlations between participant’s performances were sufficiently large for PCA.

TABLE 10. KMO VALUES FOR ALL PARTICIPANTS FOR THE Y-AXIS (NFH CONDITION). VALUES FOR INDIVIDUAL PARTICIPANTS ARE HIGHLIGHTED IN GREY (SIGNIFICANT > 0.5).

Anti-image Matrices

		P1	P2	P3	P4	P5	P6	P7	P8	P9	P10	P11	P12	P13	P14	P15	P16
Anti-image Correlation	P1	.689[a]	.001	-.648	-.403	-.604	-.342	-.579	.514	.199	.212	.424	.616	-.335	.570	-.313	-.415
	P2	.001	.969[a]	-.350	-.095	-.358	.048	.016	.183	-.062	.053	-.151	.113	-.228	-.047	.187	-.005
	P3	-.648	-.350	.912[a]	.114	.399	.141	.153	-.294	-.144	-.350	.012	-.280	-.127	-.160	.287	.235
	P4	-.403	-.095	.114	.776[a]	.091	.368	.636	-.570	-.772	.524	.116	-.903	.256	-.526	.035	.726
	P5	-.604	-.358	.399	.091	.896[a]	-.086	.124	-.294	-.003	-.226	-.588	-.296	.382	-.177	.059	.285
	P6	-.342	.048	.141	.368	-.086	.862[a]	.101	-.809	-.319	.323	.247	-.563	.071	-.273	.118	.321
	P7	-.579	.016	.153	.636	.124	.101	.861[a]	-.359	-.287	.031	-.144	-.573	.301	-.734	.279	.317
	P8	.514	.183	-.294	-.570	-.294	-.809	-.359	.823[a]	.445	-.336	-.092	.701	-.129	.488	-.250	-.467
	P9	.199	-.062	-.144	-.772	-.003	-.319	-.287	.445	.820[a]	-.492	-.431	.734	.301	.170	-.109	-.864
	P10	.212	.053	-.350	.524	-.226	.323	.031	-.336	-.492	.894[a]	.231	-.363	.101	.138	-.462	.375
	P11	.424	-.151	.012	.116	-.588	.247	-.144	-.092	-.431	.231	.906[a]	-.072	-.630	.225	.018	.129
	P12	.616	.113	-.280	-.903	-.296	-.563	-.573	.701	.734	-.363	-.072	.765[a]	-.281	.511	-.080	-.788
	P13	-.335	-.228	-.127	.256	.382	.071	.301	-.129	.301	.101	-.630	-.281	.904[a]	-.207	-.454	.031
	P14	.570	-.047	-.160	-.526	-.177	-.273	-.734	.488	.170	.138	.225	.511	-.207	.837[a]	-.698	-.068
	P15	-.313	.187	.287	.035	.059	.118	.279	-.250	-.109	-.462	.018	-.080	-.454	-.698	.906[a]	-.133
	P16	-.415	-.005	.235	.726	.285	.321	.317	-.467	-.864	.375	.129	-.788	.031	-.068	-.133	.823[a]

a. Measures of Sampling Adequacy(MSA)

Lastly, for the z-axis an oblique rotation (promax) was used for the PCA with 16 participants. Eigenvalues for one component was over Kaiser’s criterion of 1 and in combination explained 99.37% of the variance. The scree plot (see Figure 24) showed inflexions that will justify retaining point three (two components) in the final analysis. Kaiser-Meyer-Olkin measure verified the sampling adequacy for the analysis, KMO= .87 (‘great’ according to Field, 2009), and as shown by Table 11, all KMO values for individual participants were > .769, which is well above the acceptable limit of 0.5 (Field, 2009). Bartlett’s test of sphericity χ^2 (120) = 173940.78, p < .001, indicated that correlations between participant’s performances were sufficiently large for PCA. An initial analysis was run to obtain eigenvalues for each component in the data.

TABLE 11. KMO VALUES FOR ALL PARTICIPANTS FOR THE Z-AXIS (NFH CONDITION). VALUES FOR INDIVIDUAL PARTICIPANTS ARE HIGHLIGHTED IN GREY (SIGNIFICANT > 0.5).

Anti-image Matrices

		P1	P2	P3	P4	P5	P6	P7	P8	P9	P10	P11	P12	P13	P14	P15	P16
Anti-image Correlation	P1	.909[a]	.216	.024	.148	.054	-.953	.060	-.103	-.066	-.205	-.411	.037	.288	.073	.090	.028
	P2	.216	.900[a]	.283	.157	-.199	-.282	-.293	.055	-.152	.038	-.223	.547	.106	-.345	.605	.093
	P3	.024	.283	.871[a]	-.094	-.105	-.017	.202	.168	-.489	-.170	.295	.154	.199	-.227	.322	.458
	P4	.148	.157	-.094	.854[a]	.663	-.423	.233	-.854	-.138	.118	-.455	.456	.154	.246	-.249	.422
	P5	.054	-.199	-.105	.663	.906[a]	-.207	.218	-.801	-.219	-.109	-.069	-.102	-.052	.066	-.192	.082
	P6	-.953	-.282	-.017	-.423	-.207	.879[a]	-.075	.305	.038	.185	.515	-.231	-.259	-.193	-.036	-.149
	P7	.060	-.293	.202	.233	.218	-.075	.854[a]	-.543	-.567	.245	-.087	.115	.679	-.109	-.461	.753
	P8	-.103	.055	.168	-.854	-.801	.305	-.543	.832[a]	.325	-.196	.358	-.278	-.335	-.089	.376	-.480
	P9	-.066	-.152	-.489	-.138	-.219	.038	-.567	.325	.892[a]	-.010	-.239	.024	-.506	.491	-.192	-.469
	P10	-.205	.038	-.170	.118	-.109	.185	.245	-.196	-.010	.769[a]	-.482	.037	.344	-.232	-.509	.276
	P11	-.411	-.223	.295	-.455	-.069	.515	-.087	.358	-.239	-.482	.855[a]	-.367	-.311	-.210	.539	-.332
	P12	.037	.547	.154	.456	-.102	-.231	.115	-.278	.024	.037	-.367	.910[a]	.089	.360	.053	.565
	P13	.288	.106	.199	.154	-.052	-.259	.679	-.335	-.506	.344	-.311	.089	.862[a]	-.466	-.183	.516
	P14	.073	-.345	-.227	.246	.066	-.193	-.109	-.089	.491	-.232	-.210	.360	-.466	.920[a]	-.343	.101
	P15	.090	.605	.322	-.249	-.192	-.036	-.461	.376	-.192	-.509	.539	.053	-.183	-.343	.866[a]	-.407
	P16	.028	.093	.458	.422	.082	-.149	.753	-.480	-.469	.276	-.332	.565	.516	.101	-.407	.844[a]

a. Measures of Sampling Adequacy(MSA)

d. Featureless night without haptic

The scree plots below (Figure 25) show the point of inflexion for X, Y, and Z that allowed the extracting of the components for the PCA.

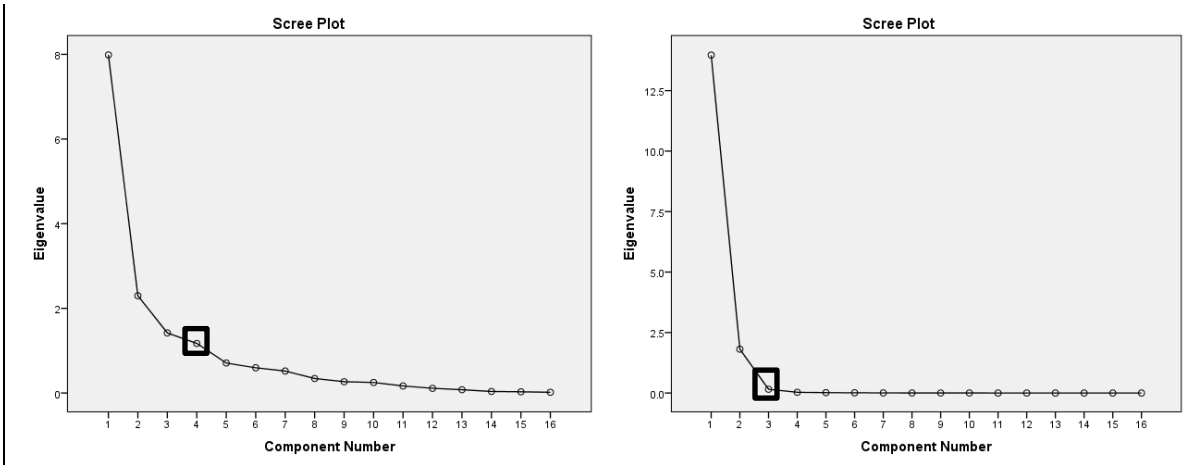

a b

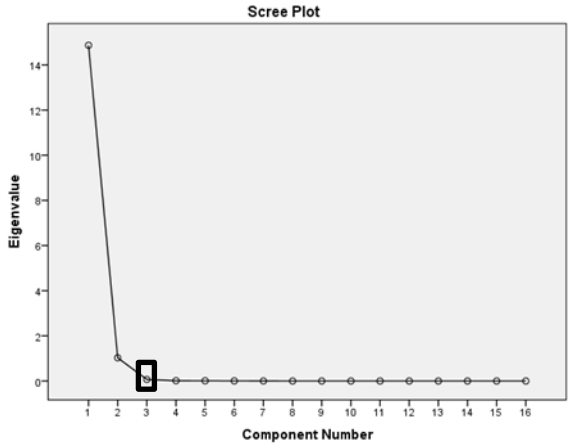

c

FIGURE 25. SCREE PLOTS SHOWING THE INFLECTION POINT (SHOWN BY THE SQUARE) FOR A) X, B) Y, AND C) Z DIRECTIONS FOR THE NFWH CONDITION.

The PCA analyses were completed for 16 participants for the mediolateral direction. The Kaiser-Meyer-Olkin measure verified adequacy for the analysis, KMO= .765 ('good' according to Field, 2009), and as shown by Table 12, all KMO values for individual participants were > .556, which is well above the acceptable limit of 0.5 (Field, 2009). Bartlett's test of sphericity χ^2 (120) = 40605.371, $p < .001$, indicated that correlations between participant's performances were sufficiently large for PCA. An initial analysis was run to obtain eigenvalues for each component in the data. Three components had eigenvalues over Kaiser's criterion of 1 and in combination explained 73.15% of the variance. For the final analysis, the scree plot (see Figure 25a) shows inflexions that will justify retaining three components.

TABLE 12. KMO VALUES FOR ALL PARTICIPANTS FOR THE X-AXIS (NFWH CONDITION). VALUES FOR INDIVIDUAL PARTICIPANTS ARE HIGHLIGHTED IN GREY (SIGNIFICANT > 0.5).

Anti-image Matrices

		P1	P2	P3	P4	P5	P6	P7	P8*	P9**	P10**	P11	P12*	P13	P14	P15	P16*
Anti-image Correlation	P1	.662[a]	-.184	-.135	-.003	.031	.086	.083	.273	-.061	-.063	-.204	.066	-.051	.086	-.011	.366
	P2	-.184	.893[a]	.126	.120	-.073	-.051	-.272	-.021	-.121	-.030	.046	.232	-.103	.108	.252	-.014
	P3	-.135	.126	.874[a]	-.313	.228	-.112	-.092	-.258	.145	.012	.225	.221	.012	-.134	.193	.103
	P4	-.003	.120	-.313	.841[a]	.032	-.236	-.267	-.330	-.521	-.091	-.361	.127	.225	.102	-.351	.151
	P5	.031	-.073	.228	.032	.759[a]	.034	.167	-.389	-.327	-.259	.345	.630	-.190	.201	.213	.262
	P6	.086	-.051	-.112	-.236	.034	.712[a]	-.044	-.131	-.117	-.580	.193	.345	-.445	.636	.444	.064
	P7	.083	-.272	-.092	-.267	.167	-.044	.900[a]	.247	-.209	-.313	.115	.050	.132	-.295	.272	-.126
	P8	.273	-.021	-.258	-.330	-.389	-.131	.247	.556[a]	.203	.106	-.294	-.292	.222	-.204	.082	-.184
	P9	-.061	-.121	.145	-.521	-.327	-.117	-.209	.203	.733[a]	.552	-.138	-.589	-.099	-.319	-.414	-.296
	P10	-.063	-.030	.012	-.091	-.259	-.580	-.313	.106	.552	.768[a]	-.075	-.464	-.132	-.361	-.492	-.086
	P11	-.204	.046	.225	-.361	.345	.193	.115	-.294	-.138	-.075	.770[a]	.449	-.517	.382	.225	.019
	P12	.066	.232	.221	.127	.630	.345	.050	-.292	-.589	-.464	.449	.647[a]	-.370	.587	.548	.384
	P13	-.051	-.103	.012	.225	-.190	-.445	.132	.222	-.099	-.132	-.517	-.370	.791[a]	-.708	-.099	-.053
	P14	.086	.108	-.134	.102	.201	.636	-.295	-.204	-.319	-.361	.382	.587	-.708	.718[a]	.213	.143
	P15	-.011	.252	.193	-.351	.213	.444	.272	.082	-.414	-.492	.225	.548	-.099	.213	.733[a]	.091
	P16*	.366	-.014	.103	.151	.262	.064	-.126	-.184	-.296	-.086	.019	.384	-.053	.143	.091	.767[a]

a. Measures of Sampling Adequacy(MSA)

For the superior-proximal direction, the PCA of the 16 participants showed that the Bartlett's test of sphericity χ^2 (120) = 203617.68, $p < .001$, indicated that correlations between participant's performances were sufficiently large while the Kaiser-Meyer-Olkin measure verified the sampling adequacy for the analysis, KMO= .85 ('great' according to Field, 2009), and as shown by Table 13, all KMO values for individual participants were > .608, which is well above the acceptable limit of 0.5 (Field, 2009). For this analysis two components had eigenvalues over Kaiser's criterion of 1 and in combination explained 98.62% of the variance. The scree plot (see Figure 25b) showed inflexions that will justify retaining two components that were retained in the final analysis.

TABLE 13. KMO VALUES FOR ALL PARTICIPANTS FOR THE Y-AXIS (NFWH CONDITION). VALUES FOR INDIVIDUAL PARTICIPANTS ARE HIGHLIGHTED IN GREY (SIGNIFICANT > 0.5).

Anti-image Matrices

		P1	P2	P3	P4	P5	P6	P7	P8	P9	P10	P11	P12	P13	P14	P15	P16
Anti-image Correlation	P1	.608[a]	-.457	-.750	.064	.058	.102	.171	-.373	-.480	.032	-.218	.108	.192	.444	.095	.225
	P2	-.457	.849[a]	.040	-.448	.047	-.191	-.324	.470	.107	.282	.615	-.573	-.813	-.047	-.134	-.209
	P3	-.750	.040	.872[a]	-.231	.082	.128	-.210	.388	.531	-.153	-.016	.116	.185	-.570	-.093	-.235
	P4	.064	-.448	-.231	.818[a]	-.301	-.007	.315	-.819	-.033	.084	-.362	.333	.321	.398	-.137	.458
	P5	.058	.047	.082	-.301	.913[a]	.284	-.681	-.142	-.288	.264	.336	-.461	.041	-.037	-.199	-.020
	P6	.102	-.191	.128	-.007	.284	.897[a]	-.658	-.081	-.546	.497	-.056	-.329	.025	.172	-.236	.163
	P7	.171	-.324	-.210	.315	-.681	-.658	.828[a]	-.123	.354	-.638	-.434	.639	.377	-.154	.392	.011
	P8	-.373	.470	.388	-.819	-.142	-.081	-.123	.855[a]	.266	-.222	.264	-.174	-.348	-.560	.223	-.513
	P9	-.480	.107	.531	-.033	-.288	-.546	.354	.266	.880[a]	-.297	-.027	.295	.065	-.512	-.274	.082
	P10	.032	.282	-.153	.084	.264	.497	-.638	-.222	-.297	.826[a]	.364	-.512	-.570	.561	-.696	.255
	P11	-.218	.615	-.016	-.362	.336	-.056	-.434	.264	-.027	.364	.836[a]	-.833	-.736	-.043	-.137	-.348
	P12	.108	-.573	.116	.333	-.461	-.329	.639	-.174	.295	-.512	-.833	.816[a]	.704	-.040	.279	.019
	P13	.192	-.813	.185	.321	.041	.025	.377	-.348	.065	-.570	-.736	.704	.820[a]	-.264	.272	.118
	P14	.444	-.047	-.570	.398	-.037	.172	-.154	-.560	-.512	.561	-.043	-.040	-.264	.870[a]	-.273	.355
	P15	.095	-.134	-.093	-.137	-.199	-.236	.392	.223	-.274	-.696	-.137	.279	.272	-.273	.882[a]	-.685
	P16	.225	-.209	-.235	.458	-.020	.163	.011	-.513	.082	.255	-.348	.019	.118	.355	-.685	.894[a]

a. Measures of Sampling Adequacy(MSA)

For the anterior direction (z-axis), an oblique rotation (promax) was used for the PCA. Two components had eigenvalues over Kaiser's criterion of 1 and in combination explained 99.36% of the variance. The scree plot (see Figure 25c) showed inflexions that would justify retaining two components in the final analysis. The Kaiser-Meyer-Olkin measure verified the sampling adequacy for the analysis, KMO= .86 ('great' according to Field, 2009), and as shown by Table 14, all KMO values for individual participants were > .614, which is well above the acceptable limit of 0.5 (Field, 2009). Bartlett's test of sphericity χ^2 (120) = 235956.10, $p < .001$, indicated that correlations between participant's performances were sufficiently large for PCA.

TABLE 14. KMO VALUES FOR ALL PARTICIPANTS FOR THE Z-AXIS (NFWH CONDITION). VALUES FOR INDIVIDUAL PARTICIPANTS ARE HIGHLIGHTED IN GREY (SIGNIFICANT > 0.5).

Anti-image Matrices

		P1	P2	P3	P4	P5	P6	P7	P8	P9	P10	P11	P12	P13	P14	P15	P16
Anti-image Correlation	P1	.920[a]	.426	-.060	.094	.059	.019	-.136	-.416	-.108	.254	-.185	-.400	-.328	.320	.537	-.196
	P2	.426	.614[a]	.530	-.236	.047	.137	-.274	-.542	.450	-.305	.010	-.107	-.337	.304	.541	-.247
	P3	-.060	.530	.849[a]	-.670	-.082	.041	.223	.215	.921	-.213	.280	.427	.500	-.318	-.188	-.001
	P4	.094	-.236	-.670	.808[a]	.545	-.526	-.074	-.358	-.712	-.200	-.257	-.475	-.651	.593	.164	-.644
	P5	.059	.047	-.082	.545	.890[a]	-.927	-.045	-.108	-.094	-.041	-.099	-.102	-.145	.133	.076	-.676
	P6	.019	.137	.041	-.526	-.927	.899[a]	-.202	-.121	.084	.021	.042	.023	-.031	.011	.087	.571
	P7	-.136	-.274	.223	-.074	-.045	-.202	.933[a]	.551	.048	-.187	-.081	.286	.403	-.398	-.175	.038
	P8	-.416	-.542	.215	-.358	-.108	-.121	.551	.820[a]	.152	.243	.048	.246	.779	-.727	-.735	.442
	P9	-.108	.450	.921	-.712	-.094	.084	.048	.152	.852[a]	-.087	.381	.422	.534	-.355	-.194	.039
	P10	.254	-.305	-.213	-.200	-.041	.021	-.187	.243	-.087	.957[a]	-.079	-.057	.382	-.180	-.163	.235
	P11	-.185	.010	.280	-.257	-.099	.042	-.081	.048	.381	-.079	.941[a]	.396	.266	-.487	.107	.059
	P12	-.400	-.107	.427	-.475	-.102	.023	.286	.246	.422	-.057	.396	.882[a]	.640	-.574	-.108	.143
	P13	-.328	-.337	.500	-.651	-.145	-.031	.403	.779	.534	.382	.266	.640	.764[a]	-.816	-.559	.372
	P14	.320	.304	-.318	.593	.133	.011	-.398	-.727	-.355	-.180	-.487	-.574	-.816	.818[a]	.246	-.518
	P15	.537	.541	-.188	.164	.076	.087	-.175	-.735	-.194	-.163	.107	-.108	-.559	.246	.886[a]	-.203
	P16	-.196	-.247	-.001	-.644	-.676	.571	.038	.442	.039	.235	.059	.143	.372	-.518	-.203	.873[a]

a. Measures of Sampling Adequacy(MSA)

e. Between condition analysis

The PCA analysis for each condition and each direction showed that there were not significant differences between the participants' trajectory for each single direction as depicted by the highly correlated values. We were therefore able to perform an analysis on the mean trajectory for each coordinate by averaging the results of all participants, as shown by Figure 26 for x-axis, Figure 27 for y-axis, and Figure 28 for z-axis. Correlations factors (Pearson-r^2) and their significant levels (0.4 according to Stevens, 2002 for these type of data) are shown in Table 15 and Table 18.

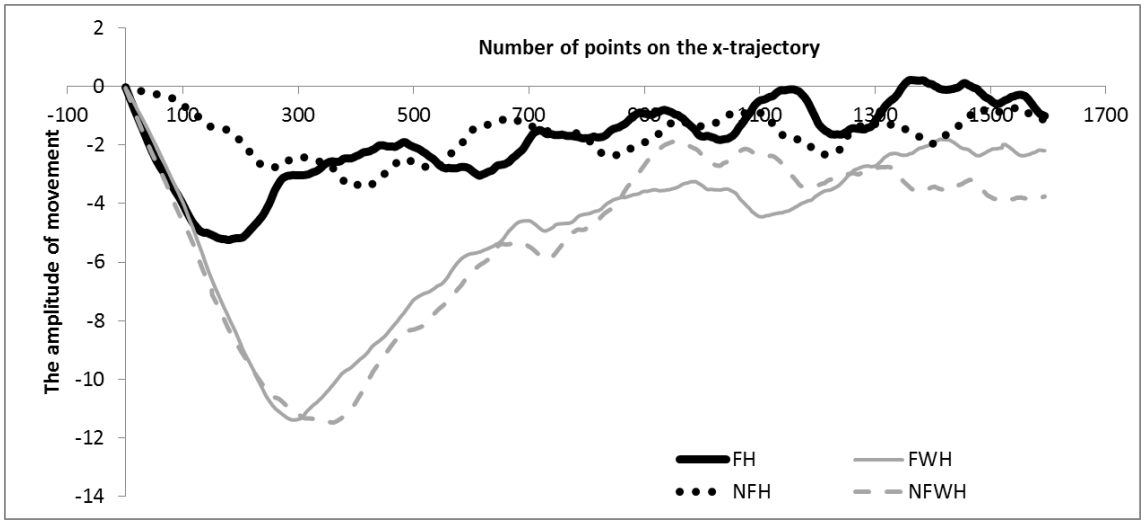

FIGURE 26. MEAN TRAJECTORY FOR EACH CONDITION (FH, FWH, NFH, AND NFWH) FOR X-AXIS.

For the mediolateral direction, as indicated by Table 15 and Figure 26, the results clearly indicate that the haptic feedback was helpful in left and right movements. The haptic feedback helped to keep the trajectory close to the center (0 line on the figures). However, the haptic feedback was less helpful in the featured night condition (FH), where the horizon was always indicated, as depicted by a significant low R-squared value (0.052) comparing to the featureless night condition (NFH). It is possible that the participants relied more on the visual feedback and adjust the haptic feedback accordingly based on the visual input; while in the featureless environment the visual feedback was clueless, which forced the participants to rely on the haptic feedback. The trajectory shift was more evident for the non-haptic condition (for both FWH and NFWH).

TABLE 15. PEARSON-R^2 VALUES FOR X-AXIS (SIGNIFICANT =.4).

Correlation Matrix[a]				
		FH	FWH	NFH
	FWH	.440		
	NFH	0.052[a]	.550	
	NFWH	.410	.900	.540

a. Significant = .4

Similarly, the haptic feedback did not affect performances for the y direction. However, Figure 27 shows that the landing at the end of the trajectory seems smoother when the haptic feedback is present. Therefore, we compared the correlation factor r^2 for the beginning and the end of the y-trajectory (shown by the grey area on Figure 27). When participants began landing, trajectories were similar for all the conditions as depicted by the higher correlated Pearson-r^2, which suggests that adding haptic feedback would not affect the up-down trajectory at the beginning of the landing (Table 16). However, the end of the landing is affected by the usage of haptics as Pearson-r^2 show significant difference between the FH and the other conditions, (Table 17). Perhaps the present findings are a result of participants relying heavily on their visual sense during the featured night conditions that had haptic feedback and did not have haptic feedback.

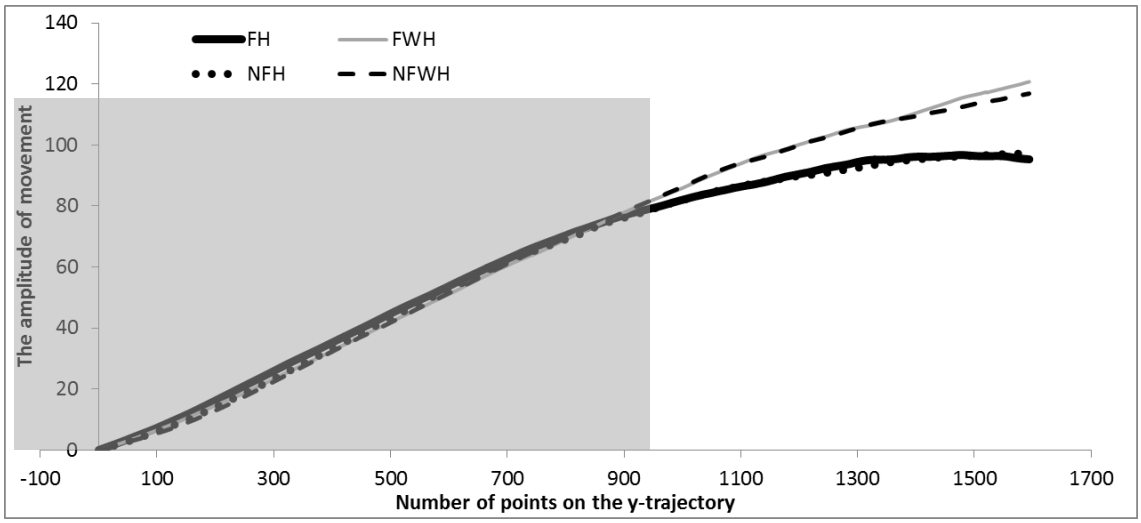

FIGURE 27. MEAN TRAJECTORY FOR EACH CONDITION (FH, FWH, NFH, AND NFWH) FOR Y-AXIS.

TABLE 16. PEARSON-R^2 VALUES FOR Y-AXIS BEGINNING OF TRAJECTORY (SIGNIFICANT =.4).

Correlation Matrix[a]				
		FH	FWH	NFH
	FWH	0.99		
	NFH	1	0.99	
	NFWH	0.992	1	0.992

a. Significant = .4

TABLE 17. PEARSON-R^2 VALUES FOR Y-AXIS END OF TRAJECTORY (SIGNIFICANT =.4).

Correlation Matrix[a]				
		FH	FWH	NFH
	FWH	0.083[a]		
	NFH	0.142[a]	0.978	
	NFWH	0.046[a]	0.992	0.958

a. Significant = .4

Finally, as expected the haptic feedback did not affect performances for the z direction, as the speed on this direction was predetermined. Figure 28 clearly shows that

the trajectories for all conditions were similar. Pearson-r^2 values show strong correlations between the four conditions (Table 18).

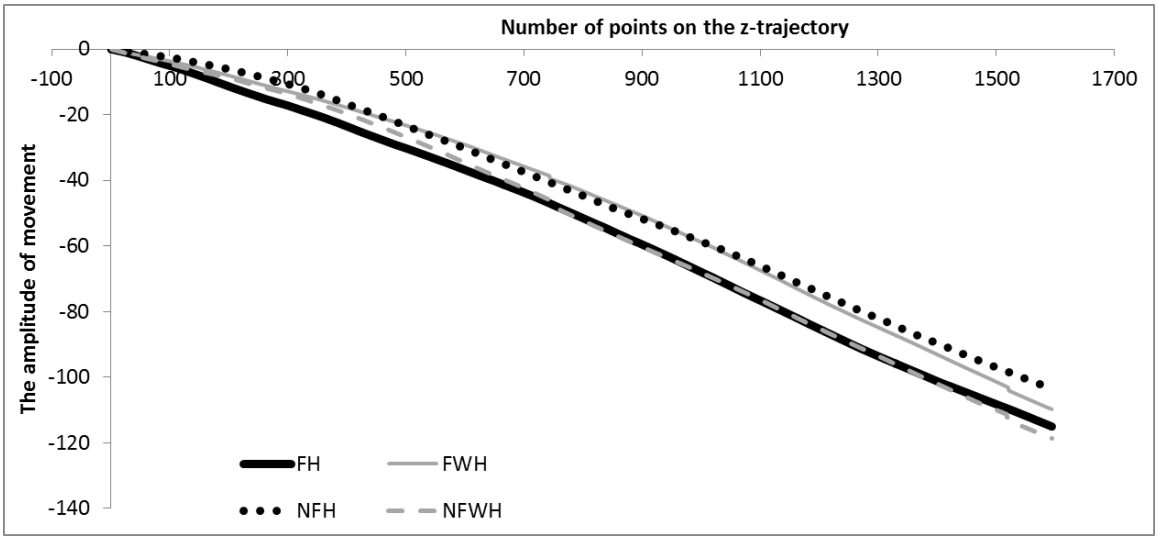

FIGURE 28. MEAN TRAJECTORY FOR EACH CONDITION (FH, FWH, NFH, NFWH) FOR Z-AXIS.

TABLE 18. PEARSON-R^2 VALUES FOR Z-AXIS (SIGNIFICANT =.4).

Correlation Matrix[a]				
		FH	FWH	NFH
	FWH	.996		
	NFH	.998	.998	
	NFWH	.998	.998	1.000

a. Significant = .4

Repeated measures ANOVA for completion time were not significant. Table 19 shows the mean values for the each condition for all the participants.

TABLE 19. MEAN TIME VALUES FOR EACH CONDITION (FH, FWH, NFH, AND NFWH).

Descriptive Statistics

	Mean	Std. Deviation	N
FH	47.11	10.01	16
FWH	50.28	10.79	16
NFH	49.00	12.02	16
NFWH	47.97	10.03	16

4. DISCUSSION

The present study showed that force feedback was efficient for landing trajectories in a featureless environment. Indeed, it helped participants to deviate less from the center of the runway when trying to land an object.

On one hand, these results confirm previous findings of Trlep et al. (2011) that had stroke patients complete a bimanual flying task with the HapticMaster. It was found that the motor deficient arm improved on the x-axis trajectory. Since few studies explored flying and landing as potential tasks for neurorehabilitation, further investigation are required to explore their efficiency in upper limb paralysis. Ideally, the same experiment should be replicated with people that have difficulty with their upper limb movements.

On the other hand and to our knowledge, this is the first investigation of the black hole illusion in the haptic modality. Since haptic feedback tends to improved landing trajectories in featureless environment, our findings could benefit flying and landing studies and further investigation is required. For instance, the VE should be improved to resemble airplane displays. The runway lights should be also incorporated. Finally, the z-trajectory should be dependent on the users' movements and not predetermined by the software. For instance, the night landing conditions presented in this thesis could be modified by incorporating conditions with different speeds or asking the participants to

perform the task in a specific timeframe. Modifying the speed and the time could offer insight on landing task and therefore suggest alternative solution to reduce BHI.

In the future and if deemed feasible, recruiting patients with upper limb paralysis could be beneficial. One possibility is to compare their brain activity before and after the training sessions using functional near-infrared spectroscopy (fNIRS) multimodal technique, as research showed that haptic devices along with VR could increase neuronal plasticity in patients (Takahashi et al., 2008; & Carpi, Mannini,& De Rossi, 2009).

We were not able to incorporate a tactile feedback for the scope of this thesis. However, incorporating tactile feedback along with kinesthetic feedback can provide a more effective way for treating individuals with upper limb paralysis when exploring movement trajectory for reaching tasks (Cameriao et al., 2012). In the future the same task could be extended by using braille cells (Metec AG, 2013) or ArraySense, a neck stimulation device (Tactile Image Inc., 2013).

In summary, by estimating movement trajectory, comparing pre and post motor assessments, comparing brain imagery before and after training along with OT rehabilitation training programs, it could be possible to suggest a more efficient trainings or tasks that could help patients' recovery.

5. CONCLUSION

The present thesis presented different types of haptic devices and their importance in the neurorehabilitation of upper limb paralysis patients. We explored the possibility of adding tactile feedback such as vibrations on the skin or temperature feedback to possibly stimulate the mechanoreceptors of the affected limb. The experiment suggested night landing an object on a runway could be added to the existing tasks not only for

rehabilitation purposes, by also to decrease the effect of the black hole illusion in pilots. Our study clearly showed that haptic feedback is useful in a featureless environment. However, when visual cues were present, efficiency was minimized for parts of the trajectories. That said, our major limitation was related to technical issue that did not fully allow us of the BHI. If deemed feasible, runway lights should be added in the virtual environment and the yellow target removed, as it may give indication on the horizon; although this effect could be minimal. Most importantly, haptic feedback, when an object is in contact with the ground, may be necessary to complete immersion. Finally, one of our regret is the impossibility to evaluate the effectiveness of tactile directional cues in the designed study for technical issues that prevent us to incorporate braille cells into our original design; a direction that we hoped could be explored in the future.

REFERENCES

Adamovich, S. V., Fluet, G. G., Tunik, E., & Merians, A. S. (2009). Sensorimotor training in virtual reality: A review. *NeuroRehabilitation*, *25*(1), 29–44. doi:10.3233/NRE-2009-0497

Adamovich, S. V., Merians, A. S., Boian, R., Lewis, J. A., Tremaine, M., Burdea, G. S., … Poizner, H. (2005). A virtual reality-based exercise system for hand rehabilitation post-stroke. *Presence: Teleoperators & Virtual Environments*, *14*(2), 161–174. doi:10.1.1.86.198

Balasubramanian, S., Klein, J., & Burdet, E. (2010). Robot-assisted rehabilitation of hand function. *Current Opinion in Neurology*, *23*(6), 661–670. doi:10.1097/WCO.0b013e32833e99a4

Bergamasco, M., Avizzano, C. A., Frisoli, A., Ruffaldi, E., & Marcheschi, S. (2006). Design and validation of a complete haptic system for manipulative tasks. Advanced Robotics, 20(3), 367–389. doi: 10.1163/156855306776014367

Boian, R., Sharma, A., Han, C., Merians, A., Burdea, G., Adamovich, S., … Poizner, H. (2002). Virtual reality-based post-stroke hand rehabilitation. *Studies in Health Technology and Informatics*, 64–70.

Bouzit, M., Popescu, G., Burdea, G., & Boian, R. (2002). The Rutgers Master II-ND force feedback glove. *Proceedings 10th Symposium in Haptic Interfaces for Virtual Environment and Teleoperator Systems*, 145–152. doi:10.1109/HAPTIC.2002.998952

Broeren, J., Rydmark, M., & Sunnerhagen, K. S. (2004). Virtual reality and haptics as a training device for movement rehabilitation after stroke: A single-case study. Archives of Physical Medicine and Rehabilitation, 85(8), 1247–1250. doi:10.1016/j.apmr.2003.09.020

Broeren, J., Rydmark, M., Bjorkdahl, A., & Sunnerhagen, K. S. (2007). Assessment and Training in a 3-Dimensional Virtual Environment With Haptics: A Report on 5 Cases of Motor Rehabilitation in the Chronic Stage After Stroke. Neurorehabilitation and Neural Repair, 21(2), 180–189. doi:10.1177/1545968306290774

Bulkley, N. K., Dyre, B. P., Lew, R., & Caufield, K. (2009). A peripherally-located virtual instrument landing display affords more precise control of approach path during simulated landings than traditional instrument landing displays. *Human Factors and Ergonomics Society Annual Meeting Proceedings*, *53*(1), 31–35. doi:10.1518/107118109X12524440832827

CAHAI. (2004). *The Chedoke Arm and Hand Activity Inventory Administration Manual, 2*. Retrieved from http://www.cahai.ca/manual.html

Cameirao, M. S., Badia, S. B. i., Duarte, E., Frisoli, A., & Verschure, P. F. M. J. (2012). The combined impact of virtual reality neurorehabilitation and its interfaces on upper extremity functional recovery in patients with chronic stroke. *Stroke*, *43*(10), 2720–2728. doi:10.1161/STROKEAHA.112.653196

Carpi, F., Mannini, A., & De Rossi, D. (2009). Dynamic splint-like hand orthosis for finger rehabilitation. In F. Carpi, & E. Smela (Eds.), *Biomedical Applications of Electroactive Polymer Actuators* (pp. 443-461). West Sussex: United Kingdom: John Wiley & Sons Ltd. doi:10.1002/9780470744697

Centers for Disease Control and Prevention. (2012). Traumatic Brain Injury. http://www.cdc.gov/traumaticbraininjury/statistics.html

Chiasson, J., McGrath, B. J., & Rupert, A. H. (2003). Enhanced situation awareness in sea, air and land environments. *RTO HFM Symposium on "Spatial Disorientation in Military Vehicles: Causes, Consequences and Cures*.

Christiansen, R., Contreras-Vidal, J. L., Glillespis, B. R., Shewokis, P. A., & K. O'Malley, M. (2013). Vibrotactile feedback of pose error enhances myoelectric control of a prosthetic hand. *IEEE World Haptics Conference*, 531-536. doi:10.1109/WHC.2013.6548464.

Chortis, A., Standen, P. J., & Walker, M. (2008). Virtual reality system for extremity rehabilitation of chronic stroke patients living in the community. In P. Sharkey, P. Lopes-Dos-Santos, P. L. Weiss, T. Brooks, *The 7th International Conference on Disability, Virtual Reality and Associated Technologies with ArtAbilitation*, 221-228.

Clavel R. (1990). Device for the movement and positioning of an element in space. *Google Patents*. Retrieved from http://www.google.com/patents/US4976582

CyberGlove Systems LLC. (2012). CyberForce, CyberGlove II/III, CyberGrasp, and CyberTouch, Retrieved from http://www.cyberglovesystems.com.

Demain, S., Metcalf, C. D., Merrett, G. V., Zheng, D., & Cunningham, S. (2012). A narrative review on haptic devices: Relating the physiology and psychophysical properties of the hand to devices for rehabilitation in central nervous system disorders. *Disability and Rehabilitation: Assistive Technology*, (00), 1–9. doi:10.3109/17483107.2012.697532

Dvorkin, A. Y., Zollman, F. S., Beck, K., Larson, E., & Patton, J. L. (2009). A virtual environment-based paradigm for improving attention in TBI. In, *ICORR 2009. IEEE International Conference on Rehabilitation Robotics*, pp. 962–965. doi:10.1109/ICORR.2009.5209629

Endo, T., Kawasaki, H., Mouri, T., Ishigure, Y., Shimomura, H., Matsumura, M., & Koketsu, K. (2011). Five-fingered haptic interface robot: HIRO III. *IEEE Transactions on Haptics*, *4*(1), 14–27. doi:10.1109/WHC.2009.4810812

Escolano, C., Murguialday, A. R., Matuz, T., Birbaumer, N., & Minguez, J. (2010). A telepresence robotic system operated with a P300-based brain-computer interface: Initial tests with ALS patients. *Annual International Conference of the IEEE Engineering in Medicine and Biology Society (EMBC)*, 4476–4480.

Field, A., (2009). *Discovering Statistics using SPSS* (3rd ed.). Los Angeles, CA: Sage.

Finley, M. A., Fasoli, S. E., Dipietro, L., Ohlhoff, J., MacClellan, L., Meister, C., … Hogan, N. (2005). Short-duration robotic therapy in stroke patients with severe upper-limb motor impairment. *The Journal of Rehabilitation Research and Development*, *42*(5), 683. doi:10.1682/JRRD.2004.12.0153

Foyle, D. C., Kaiser, M. K., & Johnson, W. W. (1992). Visual cues in low-level flight: Implications for pilotage, training, simulation, and enhanced/synthetic vision systems. *In American Helicopter Society 48th Annual Forum*, *1*, 253–260.

Frisoli, A., Bergamasco, M., Wu, S. L., & Ruffaldi, E. (2005). Evaluation of multipoint contact interfaces in haptic perception of shapes. Multi-Point Interaction with Real and Virtual Objects, 177–188. doi:10.1007/11429555_11

Frisoli, A., Borelli, L., Montagner, A., Marcheschi, S., Procopio, C., Salsedo, F., Bergamasco, M., Carboncini, M. C., & Rossi, B. (2008). Robotic-mediated arm rehabilitation in virtual environments for chronic stroke patients: A clinical study. *IEEE International Conference on Robotics and Automation*, 2465-2470. doi:10.1109/ROBOT.2008.4543583

Frisoli, A. (2009a). Research on Rehabilitation Robotics. *PERCRO*, Retrieved from, http://percro.sssup.it/~antony/Research.htm

Frisoli, A., Bergamasco, M., Carboncini, M. C., & Rossi, B. (2009b). Robotic assisted rehabilitation in virtual reality with the L-EXOS. *Stud Health Technol Inform*, *145*, 40–54.

Frisoli, A., Salsedo, F., Bergamasco, M., Rossi, B., & Carboncini, M. C. (2009c). A force-feedback exoskeleton for upper-limb rehabilitation in virtual reality. *Applied Bionics and Biomechanics*, *6*(2), 115–126. doi:10.1080/11762320902959250

Frisoli, A., Solazzi, M., Reiner, M., & Bergamasco, M. (2011). The contribution of cutaneous and kinesthetic sensory modalities in haptic perception of orientation. *Brain Research Bulletin*, *85*(5), 260–266. doi:10.1016/j.brainresbull.2010.11.011

Frisoli, A., Loconsole, C., Leonardis, D., Banno, F., Barsotti, M., Chisari, C., & Bergamasco, M. (2012). A new gaze-BCI-driven control of an upper limb exoskeleton for rehabilitation in real-world tasks. *IEEE Transactions on Systems, Man, and Cybernetics, Part C (Applications and Reviews), 42*(6), 1169–1179. doi:10.1109/TSMCC.2012.2226444

GeoMagic Inc., (2013). Haptic devices & toolkits. Retrieved from, http://www.geomagic.com/en/

Gibb, R. W. (2007). Visual spatial disorientation: Revisiting the black hole illusion. *Aviation, Space, and Environmental Medicine*, *78*(8), 801–808

Gladstone, D. J., Danells, C. J., & Black, S. E. (2002). The Fugl-Meyer Assessment of Motor recovery after stroke: A critical review of its measurement properties. *Neurorehabilitation and Neural Repair, 16*(3), 232–240. doi:10.1177/154596802401105171

Gomez-Rodriguez, M., Peters, J., Hill, J., Schölkopf, B., Gharabaghi, A., & Grosse-Wentrup, M. (2010a). Closing the sensorimotor loop: Haptic feedback facilitates decoding of arm movement imagery. *IEEE International Conference on Systems Man and Cybernetics (SMC)*, 121–126. , doi:10.1109/ICSMC.2010.5642217

Gomez-Rodriguez, M., Peters, J., Hill, J., Schölkopf, B., Gharabaghi, A., & Grosse-Wentrup, M. (2010b). Combining real-time brain-computer interfacing and robot control for stroke rehabilitation. *International. Conf. on Simulation, Modeling and Programing for Autonomous Robots*, 59-63.

Grunwad, M. (2008). Human Haptic Perception Basics and Applications, Basel, Switzerland: Birkhauser Verlag.

Gupta, A., & O'Malley, M. K. (2007). Robotic exoskeletons for upper extremity rehabilitation. *In Tech Education and Publishing, Vienna, Austria*, 371–396. doi:10.5772/5171.

Guidali, M., Duschau-Wicke, A., Broggi, S., Klamroth-Marganska, V., Nef, T., & Riener, R. (2011). A robotic system to train activities of daily living in a virtual environment. *Medical & Biological Engineering & Computing*, *49*(10), 1213–1223. doi:10.1007/s11517-011-0809-0

Hioki, M., Kawasaki, H., Sakaeda, H., Nishimoto, Y., & Mouri, T. (2011). Finger rehabilitation support system using a multifingered haptic interface controlled by a surface electromyogram. *Journal of Robotics*, 1–10. doi:10.1155/2011/167516

Holmes, S. R., Bunting, A., Brown, D. L., Hiatt, K. L., Braithwaite, M. G., & Harrigan, M. J. (2003). Survey of spatial disorientation in military pilots and navigators. *Aviation, Space, and Environmental Medicine, 74*(9), 957–965.

Jack, D., Boian, R., Merians, A. S., Tremaine, M., Burdea, G. C., Adamovich, S. V., … Poizner, H. (2001). Virtual reality-enhanced stroke rehabilitation. *IEEE Transactions on Neural Systems and Rehabilitation Engineering*, *9*(3), 308–318.

Jarillo-Silva, A., Domínguez-Ramírez, O. A., & Parra-Vega, V. (2010). Haptic training method for a therapy on upper limb. *3rd International Conference on Biomedical Engineering and Informatics (BMEI)*, *4*, 1750–1754. doi:10.1109/BMEI.2010.5640030

Johnson, M. J. (2006). Recent trends in robotic-assisted therapy environments to improve real-life functional performance after stroke. *Journal of NeuroEngineering and Rehabilitation*, *3*(29). doi:doi:10.1186/1743-0003-3-29

Johnson, M. J., Loureiro, R. C. V., & Harwin, W. S. (2008). Collaborative tele-rehabilitation and robot-mediated therapy for stroke rehabilitation at home or clinic. *Intelligent Service Robotics*, *1*(2), 109–121. doi:10.1007/s11370-007-0010-3

Johnson, M. J., Wang, S., Bai, P., Strachota, E., Tchekanov, G., Melbye, J., & McGuire, J. (2011). Bilateral assessment of functional tasks for robot-assisted therapy applications. *Medical & Biological Engineering & Computing*, *49*(10), 1157–1171. doi:10.1007/s11517-011-0817-0

Krakauer, J. W. (2005). Arm function after stroke: From physiology to recovery. In *Seminars in Neurology, 25, 384–395.* doi:10.1055/s-2005-923533.

Krebs, H. I., Hogan, N., Aisen, M. L., & Volpe, B. T. (1998). Robot-aided neurorehabilitation. *IEEE Transactions on Rehabilitation Engineering*, *6*(1), 75–87. doi:10.1109/86.662623

Krebs, H. I., Ferraro, M., Buerger, S. P., Newbery, M. J., Makiyama, A., Sandmann, M., … Hogan, N. (2004). Rehabilitation robotics: pilot trial of a spatial extension for MIT-Manus. *Journal of NeuroEngineering and Rehabilitation*, *1*(1), 5. doi10.1186/1743-0003-1-5

Larson, E. B., Ramaiya, M., Zollman, F. S., Pacini, S., Hsu, N., Patton, J. L., & Dvorkin, A. Y. (2011). Tolerance of a virtual reality intervention for attention remediation in persons with severe TBI. *Brain Injury*, *25*(3), 274–281. doi:10.3109/02699052.2010.551648

Loconsole, C., Bartalucci, R., Frisoli, A., & Bergamasco, M. (2011). A new gaze-tracking guidance mode for upper limb robot-aided neurorehabilitation. *IEEE World Haptics Conference (WHC)*, 185–190.

Loconsole, C., Leonardis, D., Barsotti, M., Solazzi, M., Frisoli, A., Bergamasco, M., … Castelli, V. P. (2013). An EMG-based robotic hand exoskeleton for bilateral training of

grasp. *IEEE World Haptics Conference (WHC)*, 537–542. doi:10.1109/WHC.2013.6548465

Lo, A. C., Guarino, P. D., Richards, L. G., Haselkorn, J. K., Wittenberg, G. F., Federman, D. G., … Volpe, B. T. (2010). Robot-assisted therapy for long-term upper-limb impairment after stroke. *New England Journal of Medicine, 362*(19), 1772–1783. doi:10.1056/NEJMoa0911341

Loureiro, R., Amirabdollahian, F., Coote, S., Stokes, E., & Harwin, W. (2001). Using haptics technology to deliver motivational therapies in stroke patients: Concepts and initial pilot studies. *Proceedings of EuroHaptics*,

Loureiro, R. C. V., Amirabodollahian, F., Topping, M., & Harwin W. S. (2003). Upper limb robot mediated stroke therapy-GENTLE/s approach. *Autonomous Robots, 15*, 35-51. doi:10.1023/A:1024436732030

Loureiro, R. C. V., & Harwin, W. S. (2007). Reach & grasp therapy: Design and control of a 9-DOF robotic neuro-rehabilitation system. *IEEE 10th International Conference on Rehabilitation Robotics*, 757–763. doi:10.1109/ICORR.2007.4428510

Loureiro, R. C., Lamperd, B., Collin, C., & Harwin, W. S. (2009). Reach & grasp therapy: Effects of the Gentle/G System assessing sub-acute stroke whole-arm rehabilitation. *IEEE International Conference on Rehabilitation Robotics*, 755–760. doi:10.1109/ICORR.2009.5209509

Loureiro, R. C. V., Harwin, W. S., Nagai, K., & Johnson, M. (2011). Advances in upper limb stroke rehabilitation: A technology push. *Medical & Biological Engineering & Computing*, *49*(10), 1103–1118. doi:10.1007/s11517-011-0797-0

Lum, P. S., Burgar, C. G., Shor, P. C., Majmundar, M., & Van der Loos, M. (2002). Robot-assisted movement training compared with conventional therapy techniques for the rehabilitation of upper-limb motor function after stroke. *Archives of Physical Medicine and Rehabilitation*, *83*(7), 952–959. doi:10.1053/apmr.2001.33101

Lum, P. S., Burgar, C. G., Van der Loos, M., Shor, P. C., Majmundar, M., & Yap, R. (2005). The MIME robotic system for upper-limb neuro-rehabilitation: results from a clinical trial in subacute stroke. *In 9th International Conference on Rehabilitation Robotics*, 511–514.

Lum, P. S., Godfrey, S. B., Brokaw, E. B., Holley, R. J., & Nichols, D. (2012). Robotic approaches for rehabilitation of hand function after stroke. *American Journal of Physical Medicine & Rehabilitation, 91,* S242–S254. doi:10.1097/PHM.0b013e31826bcedb

Luo, X., Kline, T., Fischer, H. C., Stubblefield, K. A., Kenyon, R. V., & Kamper, D. G. (2005). Integration of augmented reality and assistive devices for post-stroke hand opening rehabilitation. *27th Annual International Conference of the Engineering in Medicine and Biology Society*, 6855–6858. doi:10.1109/IEMBS.2005.1616080

Luo, X., Kenyon, R., & Kamper, D. (2006). Vr post-stroke hand opening rehabilitation: An approach utilizing virtual reality, body orthosis and pneumatic device. *International Conference on Aging, Disability and Independence, 1*, 3.

Martin, S., & Hillier, N. (2009). Characterisation of the Novint Falcon haptic device for application as a robot manipulator. In *Australasian Conference on Robotics and Automation (ACRA)*, 291–292.

McDonald, J. W., & Sadowsky, C. (2004). Spinal-cord injury. *The Lancet*, *359*(9304), 417-425.

McGrath, J., Estrada, A., Braithwaite, M. G., Raj, A. K., & Rupert, A. H. (2004). Tactile situation awareness system flight demonstration final report. USAARL Report.

Merians, A. S., Jack, D., Boian, R., Tremaine, M., Burdea, G. C., Adamovich, S. V., … Poizner, H. (2002). Virtual reality–augmented rehabilitation for patients following stroke. *Physical Therapy*, *82*(9), 898–915.

Mertens, H. W., & Lewis, M. F. (1982). Effect of different runway size on pilot performance during simulated night landing approaches. *Aviation, Space, and Environmental Medicine, 53*(5). 463-471.

Metec AG. (2013). Braille Cells. Retrieved from http://web.metec-ag.de/braille%20cells.html

Mihelj, M., Podobnik, J., & Munih, M. (2008). HEnRiE-haptic environment for reaching and grasping exercise. *2nd IEEE International Conference on Biomedical Robotics and Biomechatronics*, 907–912. doi:10.1109/BIOROB.2008.4762810

Miller, E. L., Murray, L., Richards, L., Zorowitz, R. D., Bakas, T., Clark, P., … (2010). Comprehensive overview of nursing and interdisciplinary rehabilitation care of the stroke patient: A scientific statement from the American Heart Association. *Stroke*, *41*(10), 2402–2448. doi:10.1161/STR.0b013e3181e7512b

Nagaraj, S. B., & Constantinescu, D. (2009). Effect of Haptic Force Feedback on Upper Limb. *2nd International Conference on Emerging Trends in Engineering and Technology (ICETET)*, 55–58. doi: 10.1109/ICETET.2009.85

National Stroke Association, (2012). What is stroke. Retrieved from http://www.stroke.org/site/PageServer?pagename=stroke C

Nef, T., Mihelj, M., & Riener, R. (2007). ARMin: A robot for patient-cooperative arm therapy. *Medical & Biological Engineering & Computing*, *45*(9), 887–900. doi:10.1007/s11517-007-0226-6

O'Malley, M. K., Sledd, A., Gupta, A., Patoglu, V., Huegel, J., & Burgar, C. (2006). The RiceWrist: A distal upper extremity rehabilitation robot for stroke therapy. In *ASME International Mechanical Engineering Congress and Exposition*. 1437- 1446.

Pak, S., & Patten, C. (2008). Strengthening to promote functional recovery poststroke: An evidence-based review. *Topics in Stroke Rehabilitation*, *15*(3), 177–199. doi:10.1310/tsr1503-177

Pehlivan, A. U., Lee, S., & O'Malley, M. K. (2012). Mechanical design of RiceWrist-S: A forearm-wrist exoskeleton for stroke and spinal cord injury rehabilitation. *In 4th IEEE RAS & EMBS International Conference on Biomedical Robotics and Biomechatronics (BioRob)*, 1573–1578. doi:10.1109/BioRob.2012.6290912

Podobnik, J., Mihelj, M., & Munih, M. (2009). Upper limb and grasp rehabilitation and evaluation of stroke patients using HenRiE device. *In Virtual Rehabilitation International Conference*, 173–178. doi:10.1109/ICVR.2009.5174227

Podobnik, J., Novak, D., & Munih, M. (2011). Grasp coordination in virtual environments for robot-aided upper extremity rehabilitation. *Biomedical Engineering: Applications, Basis and Communications*, *23*(06), 457–466. doi:10.4015/S1016237211002876

PURE FORM. (2004). The museum of PURE FORM. *PERCRO*, Retrieved from http://www.pureform.org/

Rehabilitation Institute of Chicago. Rehabilitation measures database. Retrieved from http://www.rehabmeasures.org/default.aspx. 2010

Reeve Foundation (2013). Paralysis facts and figures. Retrieved from http://www.christopherreeve.org/site/c.mtKZKgMWKwG/b.5184189/k.5587/Paralysis_Facts__Figures.html

Reiner, M., Halevy, G., Hecht, D., Furman, M., & Vainsencher, D. (2004). Discrimination among three types of anomalies in a visual-haptic virtual environment. *Presence, 13*(50) 317-320.

Reinkensmeyer, D. J., Emken, J. L., & Cramer, S. C. (2004). Robotics, motor learning, and neurologic recovery. *Annual Review of Biomedical Engineering*, *6*(1), 497–525. doi:10.1146/annurev.bioeng.6.040803.140223

Rizzo, A., McLaughlin, M., Jung, Y., Peng, W., Yeh, S.-C., & Zhu, W. (2005). Virtual therapeutic environments with haptics: An interdisciplinary approach for developing post-stroke rehabilitation systems. *Proc. Computers for People with Special Needs*, 70–76.

Rossini, P. M., Micera, S., Benvenuto, A., Carpaneto, J., Cavallo, G., Citi, L., … Di Pino, G. (2010). Double nerve intraneural interface implant on a human amputee for robotic hand control. *Clinical Neurophysiology*, *121*(5), 777–783. doi:10.1016/j.clinph.2010.01.001

Rozario, S. V., Housman, S., Kovic, M., Kenyon, R. V., & Patton, J. L. (2009). Therapist-mediated post-stroke rehabilitation using haptic/graphic error augmentation. *Annual International Conference of the IEEE Engineering in Medicine and Biology Society*, 1151–1156.

Sanchez, R. J., Liu, J., Rao, S., Shah, P., Smith, R., Rahman, T., … Reinkensmeyer, D. J. (2006). Automating arm movement training following severe stroke: functional exercises with quantitative feedback in a gravity-reduced environment. *IEEE Transactions on Neural Systems and Rehabilitation Engineering*, *14*(3), 378–389.

SensAble Technologies Inc., (2012). PHANToM OMNI, DeskTop, Premium 1.5, and Premium 3.0. Retrieved from http://www.sensable.com.

Shadmehr, R., & Brashers-Krug, T. (1997). Functional stages in the formation of human long-term motor memory. *The Journal of Neuroscience*, *17*(1), 409–419. doi:10.1007/s002210100787

Sledd, A., & O'Malley, M. K. (2006). Performance enhancement of a haptic arm exoskeleton. *14th Symposium on Haptic Interfaces for Virtual Environment and Teleoperator Systems*, 375–381. doi:10.1109/HAPTIC.2006.1627127

Steffin, M. (1997). Virtual reality therapy of multiple sclerosis and spinal cord injury: Design considerations for a haptic-visual interface. In Riva, G., Wiederhold, B., Molinari, E., & Wiederhold, B. K. (eds.), *Virtual Reality in Neuro-Psycho-Physiology: Cognitive, Clinical and Methodological Issues in Assessment and Rehabilitation*, *44*, 185-208. Amsterdam: IOS Press.

Stevens, J. P. (2002). *Applied multivariate statistics for the social sciences* (4th ed.). Hillsdale, NJ: Erlbaum.

Stienen, A. H., McPherson, J. G., Schouten, A. C., & Dewald, J. P. (2011). The ACT-4D: A novel rehabilitation robot for the quantification of upper limb motor impairments following brain injury. *IEEE International Conference Rehabilitation Robotics*, 1–6. doi:10.1109/ICORR.2011.5975460

Subramanian, S., Knaut, L. A., Beaudoin, C., McFadyen, B. J., Feldman, A. G., & Levin, M. F. (2007). Virtual reality environments for post-stroke arm rehabilitation. *Journal of Neuroengineering and Rehabilitation*, *4*(1), 20. doi: 10.1186/1743-0003-4-20

Sukal, T. M., Ellis, M. D., & Dewald, J. P. (2006). Source of work area reduction following hemiparetic stroke and preliminary intervention using the ACT 3D system. *28th Annual International Conference of the Engineering in Medicine and Biology Society*, 177–180.

Tactile Image Inc. (2013). ArraySense. Retrieved from http://www.tactileimage.com/

Takahashi, C. D., Der-Yeghiaian, L., Le, V. H., & Cramer, S. C. (2005). A robotic device for hand motor therapy after stroke. *9th International Conference on Rehabilitation Robotics*, 17–20. doi:10.1109/ICORR.2005.1501041

Tatemichi, T. K., Desmond, D. W., Stern, Y., Paik, M., Sano, M., & Bagiella, E. (1994). Cognitive impairment after stroke: frequency, patterns, and relationship to functional abilities. *Journal of Neurology, Neurosurgery & Psychiatry*, *57*(2), 202–207. doi:10.1136/jnnp.57.2.202

Taub, E., Morris, D. M., Crago, J., King, D. K., Bowman, M., Bryson, C., … Shaw, S. E. (2011). Wolf Motor Function Test (WMFT) Manual. Retrieved from http://www.uab.edu/citherapy/images/pdf_files/CIT_Training_WMFT_Manual.pdf

The Internet Stroke Center. (2013). *Barthel Index*. Retrieved from http://www.strokecenter.org/professionals/stroke-diagnosis/stroke-assessment-scales/

The Merck Manual. (2013). Physical therapy. Retrieved from http://www.merckmanuals.com/professional/special_subjects/rehabilitation/physical_therapy_pt.html

Thompson, R. C. (2009). The "black hole" night visual approach: calculated approach paths resulting from flying a constant visual vertical angle to level and upslope runways. *The International Journal of Aviation Psychology*, *20*(1), 59–73. doi:10.1080/10508410903415989

Tonelo, C. (2013). MIME rehab. *Prezi Presentation*, Retrieved from http://prezi.com/rjmijrs65esp/mime_rehab/

Trlep, M., Mihelj, M., Puh, U., & Munih, M. (2011). Rehabilitation robot with patient-cooperative control for bimanual training of hemiparetic subjects. *Advanced Robotics*, *25*(15), 1949–1968. doi:10.1163/016918611X588853

Van der Linde, R. Q., Lammertse, P., Frederiksen, E., & Ruiter, B. (2002). The HapticMaster, a new high-performance haptic interface. *In Proc. Eurohaptics*, 1-5.

Van Erp, J. B. F., Groen, E. L., Bos, J. E., & van Veen, H. A. H. C. (2006). A tactile cockpit instrument supports the control of self-motion during spatial disorientation. *The Journal of the Human Factors and Ergonomics Society*, *48*(2), 219–228. doi:10.1518/001872006777724435

Verschuren, T. A. C. (2008). Friction compensation for a haptic manipulator: The HapticMASTER. Retrieved from http://www.mate.tue.nl/mate/pdfs/8827.pdf

Viau, A., Feldman, A. G., McFadyen, B. J., & Levin, M. F. (2004). Reaching in reality and virtual reality: A comparison of movement kinematics in healthy subjects and in adults with hemiparesis. *Journal of Neuroengineering and Rehabilitation, 1*(11). doi:doi:10.1186/1743-0003-1-11

Volpe, B. T., Krebs, I., Hogan, N., Edlstein, Diels, C., Aisen, M. (2000). A novel approach to stroke rehabilitation: Robot-aided sensorimotor stimulation. *Neurology, 54*(10), 1938-1944.

Watson, D. (1992). Illusion: The last thing needed on approach and landing. *CSS Aviation Bulletin*.

Wisneski, K. J., & Johnson, M. J. (2006). Insights into modeling functional trajectories for robot-mediated daily living exercise environments. *International Conference on Biomedical Robotics and Biomechatronics,* 99–104. doi:10.1109/BIOROB.2006.1639067

Yozbatiran, N., Berliner, J., O'Malley, M., Pehlivan, A., Kadivar, Z., Boake, C., & Francisco, G. (2012). Robotic training and clinical assessment of upper extremity movements after spinal cord injury: A single case report. *Journal of Rehabilitation Medicine, 44*(2), 186–188. doi:10.2340/16501977-0924

Ziherl, J., Novak, Olensek, A., & Munih, M. (2010). Assistance in virtual environments for motor rehabilitation. In Kappers, A. M. L., van Erp, J. B. F., Bergmann-Tiest W.M., & van der Helm, F. C. T. (eds.), *Haptics Generating and Perceiving Tangible Sensations,* (117-122). Springer, New York.

APPENDIX A: PYTHON SCRIPTS FOR FEATURED HAPTICS

```
X3D profile='Immersive' version='3.0'>
<IMPORT inlineDEF="H3D_EXPORTS" exportedDEF="HDEV" AS="HDEV" />
 <Scene>
  <Group>
   <Viewpoint position="0 .4 1"/>
   <DynamicTransform DEF="G" position="0 0 -6" momentum="0 0 0">
                        <Shape>
                                <Appearance>
                                 <Material DEF="MyMaterial" diffuseColor="0 250 0" transparency="0.5" />
                                 <SmoothSurface stiffness="0"/>
                                </Appearance>
                                <Box DEF="landing" size="100 0.002 300"/>
                        </Shape>
                        <Shape>
                                <Appearance>
                                 <Material DEF="MyMaterial" diffuseColor="1 1 1"/>
                                 <SmoothSurface stiffness="0"/>
                                </Appearance>
                                <Box size=".3 .005 3"/>
                        </Shape>
                        <Shape>
                                <Appearance>
                                 <Material DEF="MyMaterial" diffuseColor="1 1 1"/>
                                 <SmoothSurface stiffness="0"/>
                                </Appearance>
                                <Box size=".3 .005 3"/>
                        </Shape>
                        <Shape>
                                <Appearance>
                                 <Material DEF="MyMaterial" diffuseColor="1 1 0"/>
                                 <SmoothSurface stiffness="0"/>
                                </Appearance>
```

```
                                    <Box size=".1 .05 .1"/>
                                </Shape>
                        </DynamicTransform>
                        <DynamicTransform DEF="B1" position = "0.7 0.0 0.0" momentum="0 0 0">
                         <Shape>
      <Appearance>
       <Material DEF="MyMaterial" diffuseColor="1 1 1" transparency="1.0"/>
       <SmoothSurface stiffness="20"/>
      </Appearance>
                                <Box size="1 10 19"/>
    </Shape>
                 </DynamicTransform>
                <DynamicTransform DEF="B2" position="-0.7 0 0" momentum="0 0 0">
                 <Shape DEF="S">
      <Appearance>
       <Material DEF="M" diffuseColor="1 1 1" transparency="1.0"/>
       <SmoothSurface stiffness="20"/>
      </Appearance>
                                <Box size="1 10 19"/>
    </Shape>
                 </DynamicTransform>
                </Group>
<MouseSensor DEF="mouse"/>
<KeySensor DEF="keyboard"/>
 <PythonScript DEF="PS" url="script.py">
   <Shape USE="S" containerField="references" />
   <Material USE="M" containerField="references" />
</PythonScript>
<ROUTE fromNode="keyboard" fromField="actionKeyPress" toNode="PS" toField="direction"/>
<ROUTE fromNode= "HDEV" fromField="trackerPosition" toNode="PS" toField="position"/>
<ROUTE fromNode="PS" fromField="position" toNode="B1" toField="momentum"/>
<ROUTE fromNode="PS" fromField="position" toNode="B2" toField="momentum"/>
<ROUTE fromNode="PS" fromField="position" toNode="G" toField="momentum"/>
 <ROUTE fromNode="PS" fromField="direction" toNode="B1" toField="momentum"/>
<ROUTE fromNode="PS" fromField="direction" toNode="B2" toField="momentum"/>
<ROUTE fromNode="PS" fromField="direction" toNode="G" toField="momentum"/>
<ROUTE fromNode= "landing" fromField="isTouched" toNode="PS" toField="block_touch"/>
 <ROUTE fromNode="M" fromField="diffuseColor" toNode="MyMaterial" toField="diffuseColor"/>
```

```
  </Scene>
</X3D>
```

APPENDIX B: PYTHON SCRIPTS FOR FEATURELESS WITH HAPTICS

```
<X3D profile='Immersive' version='3.0'>
<IMPORT inlineDEF="H3D_EXPORTS" exportedDEF="HDEV" AS="HDEV" />
 <Scene>
  <Group>
   <Viewpoint position="0 .4 1"/>
   <DynamicTransform DEF="G" position="0 0 -6" momentum="0 0 0">
                        <Shape>
                                <Appearance>
                                 <Material DEF="MyMaterial" diffuseColor="0 250 0" transparency="0.95" />
                                 <SmoothSurface stiffness="0"/>
                                </Appearance>
                                <Box DEF="landing_strip" size="100 0.002 300"/>
                        </Shape>
                        <Shape>
                                <Appearance>
                                 <Material DEF="MyMaterial" diffuseColor="1 1 1"/>
                                 <SmoothSurface stiffness="0"/>
                                </Appearance>
                                <Box size=".3 .005 3"/>
                        </Shape>
                        <Shape>
                                <Appearance>
                                 <Material DEF="MyMaterial" diffuseColor="1 1 0"/>
                                 <SmoothSurface stiffness="0"/>
                                </Appearance>
                                <Box size=".1 .05 .1"/>
                        </Shape>
               </DynamicTransform>

               <DynamicTransform DEF="B1" position = "0.7 0.0 0.0" momentum="0 0 0">
                <Shape>
      <Appearance>
```

```
        <Material DEF="MyMaterial" diffuseColor="1 1 1" transparency="1.0"/>
        <SmoothSurface stiffness="20"/>
       </Appearance>
                        <Box size="1 10 19"/>
     </Shape>
             </DynamicTransform>
            <DynamicTransform DEF="B2" position="-0.7 0 0" momentum="0 0 0">
             <Shape DEF="S">
       <Appearance>
        <Material DEF="M" diffuseColor="1 1 1" transparency="1.0"/>
        <SmoothSurface stiffness="20"/>
       </Appearance>
                        <Box DEF="wall1" size="1 10 19"/>
     </Shape>
             </DynamicTransform>
            </Group>
<MouseSensor DEF="mouse"/>
<KeySensor DEF="keyboard"/>
 <PythonScript DEF="PS" url="python.py">
   <Shape USE="S" containerField="references" />
   <Material USE="M" containerField="references" />
</PythonScript>
<ROUTE fromNode="keyboard" fromField="actionKeyPress" toNode="PS" toField="direction"/>
<ROUTE fromNode= "HDEV" fromField="trackerPosition" toNode="PS" toField="position"/>
<ROUTE fromNode="PS" fromField="position" toNode="B1" toField="momentum"/>
<ROUTE fromNode="PS" fromField="position" toNode="B2" toField="momentum"/>
<ROUTE fromNode="PS" fromField="position" toNode="G" toField="momentum"/>
 <ROUTE fromNode="PS" fromField="direction" toNode="B1" toField="momentum"/>
<ROUTE fromNode="PS" fromField="direction" toNode="B2" toField="momentum"/>
<ROUTE fromNode="PS" fromField="direction" toNode="G" toField="momentum"/>
<ROUTE fromNode="wall1" fromField="isTouched" toNode="PS" toField="touch"/>
 <ROUTE fromNode="M" fromField="diffuseColor" toNode="MyMaterial" toField="diffuseColor"/>
 </Scene>
</X3D>
```

APPENDIX C: INSTRUCTIONS TO PARTICIPANTS

After reading the consent form and being exposed to a force-feedback device, you will be asked to start an experiment.

1. The device in front of you is called the PHANToM OMNI: it provides force-feedback while you are interacting with a virtual environment by moving this stylus in the three dimensional space.
2. You will start first with a practice session. This allows you to familiarize with the device by moving objects around while you feel the force feedback. As you can see on the screen, this is a tower of blocks that you can interact with.
    a. To interact with the blocks you can use the buttons on the stylus to pick up blocks and move them throughout the environment
    b. You can also knock the blocks over.
3. Practice Trials: Once you feel comfortable with the device, you will complete two practice trials of the actual experiment.
    a. Your goal is to land the virtual stylus on the yellow pad in the middle of the runway. You feel the force feedback in one trial, while it will be remove in the other trial, so you will feel the difference between the two.
4. The experiment itself consists of 16 trials where your task is to land the object on the runway. The trial ends once you touch the yellow landing pad.
5. The whole experiment will take between 30 to 45 minutes to be completed.

APPENDIX D: INFORMED CONSENT FORM

NORTHERN MICHIGAN UNIVERSITY

INFORMED CONSENT STATEMENT

Title of Project: A Study Comparing Healthy and Brain Damaged Individuals in a Virtual Environment with a Haptic Device.

Investigators: Samantha R. Wagner (Master Candidate) and Dr. Mounia Ziat (Assistant Professor, Department of Psychology, NMU)

You are invited to participate in a research study. The purpose of this experiment is to study upper limb motor function in healthy and brain injured individuals. An undergraduate research assistant at Northern Michigan University will be conducting the study under the advisory of Dr. Mounia Ziat.

INFORMATION

Twenty people will be asked to participate in this experiment, which will consist of one session that is about 40 minutes. Participants may be of either gender and between the ages of 18 and 80.

- You will be seated at a computer and given the opportunity to practice with the haptic device for 1-3 minutes. You will use a haptic device that will give you information about the virtual environment you are in. The virtual real-life task will be performed using a program that allows you to interact with the environment presented to you by moving the stylus. Tasks include basic daily life activities and navigation.

RISKS

There are no known risks associated with participation in this study. If you experience any discomfort with your seating or the position relative to the controls, please notify the experimenter so that adjustments can be made to improve your comfort.

BENEFITS

There are no direct benefits to the participants other than research experience and the satisfaction of contributing to scientific knowledge. We anticipate that the scientific community will benefit from a better understanding of sensation and perception as well as a better understanding of virtual reality and haptic technologies in neurorehabilitation. Society at large also stands to benefit from the results of this study, as it will advance future haptic technologies and individuals who suffer from upper limb deficiencies caused by damage to the brain and spinal cord.

CONFIDENTIALITY

The data collected from participants will be stored on a computer in a secure lab using their initials only. The consent forms and participants' names will be stored in a locked filing cabinet in Dr. Ziat's lab separate from the coded data. Arbitrary code numbers will be used to differentiate between participants (if necessary) in any resultant publications or presentations. Only Dr. Ziat and the experimenter will have direct access to the data, consent forms, or participant lists. Material will be kept until full analysis of the data has been completed and the research has been published. All electronic files will be erased and hardcopies shredded 7 years after the completion of the study (by May 2020).

COMPENSATION

If you choose not to participate in this study, you may earn extra credit in your course in alternate ways. Please consult your instructor.

If you are a member of the Marquette community (non-student) you will receive compensation for your participation in this research.

CONTACT

If you have questions at any time about the study or the procedures, or you experience adverse effects as a result of participating in this study, you may contact the principal investigator, Mounia Ziat (mziat@nmu.edu and 227-2948) in the Department of Psychology, Northern Michigan University. This project has been reviewed and approved by the University Research Ethics Board at Northern Michigan University. If you feel you have not been treated according to the descriptions in this form, or your rights as a participant in research have been violated during the course of this project, you may contact the IRB chair (dereande@nmu.edu) and NMU's IRB administrator (tseethof@nmu.edu).

PARTICIPATION

Your participation in this study is voluntary; you may decline to participate without penalty. If you decide to participate, you may withdraw from the study at any time without penalty and without loss of benefits to which you are otherwise entitled. If you withdraw from the study before data collection is completed your data (if part of data is collected) will be returned to you or destroyed by either Dr. Mounia Ziat or the experimenter. You have the right to omit any question(s)/procedure(s) you choose.

FEEDBACK AND PUBLICATION

The results of the research may be published in journal articles, and other

scientific conferences and university colloquia. If you wish, the results of this study will be e-mailed to you no later than April 1st, 2014.

CONSENT

I have read and understand the above information. I have received a copy of this form. I agree to participate in this study.

Participant's signature_____ email _____ Date _____

Age_____ Gender_____

Investigator's signature_____ Date _____

APPENDIX E: EXCEL FILE OF DATA APPLIED TO EACH CONDITION

Beginning of the file

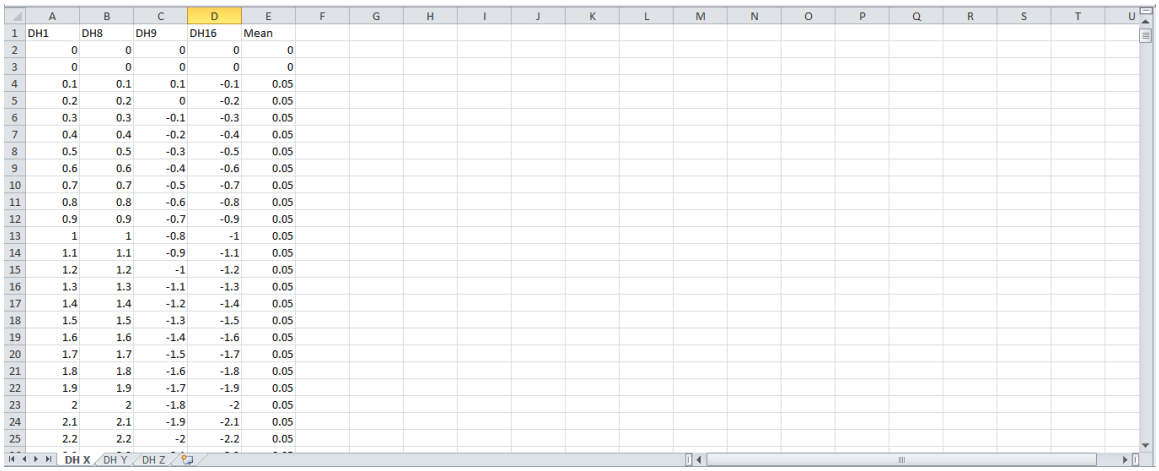

	A	B	C	D	E
1	DH1	DH8	DH9	DH16	Mean
2	0	0	0	0	0
3	0	0	0	0	0
4	0.1	0.1	0.1	-0.1	0.05
5	0.2	0.2	0	-0.2	0.05
6	0.3	0.3	-0.1	-0.3	0.05
7	0.4	0.4	-0.2	-0.4	0.05
8	0.5	0.5	-0.3	-0.5	0.05
9	0.6	0.6	-0.4	-0.6	0.05
10	0.7	0.7	-0.5	-0.7	0.05
11	0.8	0.8	-0.6	-0.8	0.05
12	0.9	0.9	-0.7	-0.9	0.05
13	1	1	-0.8	-1	0.05
14	1.1	1.1	-0.9	-1.1	0.05
15	1.2	1.2	-1	-1.2	0.05
16	1.3	1.3	-1.1	-1.3	0.05
17	1.4	1.4	-1.2	-1.4	0.05
18	1.5	1.5	-1.3	-1.5	0.05
19	1.6	1.6	-1.4	-1.6	0.05
20	1.7	1.7	-1.5	-1.7	0.05
21	1.8	1.8	-1.6	-1.8	0.05
22	1.9	1.9	-1.7	-1.9	0.05
23	2	2	-1.8	-2	0.05
24	2.1	2.1	-1.9	-2.1	0.05
25	2.2	2.2	-2	-2.2	0.05

DH X DH Y DH Z

-
-
-
-
-

End of File

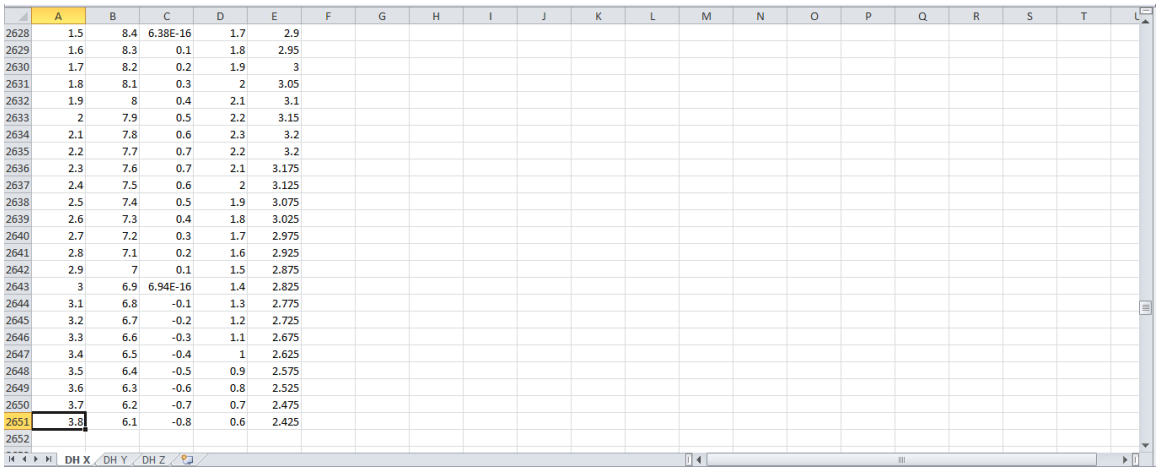

	A	B	C	D	E
2628	1.5	8.4	6.38E-16	1.7	2.9
2629	1.6	8.3	0.1	1.8	2.95
2630	1.7	8.2	0.2	1.9	3
2631	1.8	8.1	0.3	2	3.05
2632	1.9	8	0.4	2.1	3.1
2633	2	7.9	0.5	2.2	3.15
2634	2.1	7.8	0.6	2.3	3.2
2635	2.2	7.7	0.7	2.2	3.2
2636	2.3	7.6	0.7	2.1	3.175
2637	2.4	7.5	0.6	2	3.125
2638	2.5	7.4	0.5	1.9	3.075
2639	2.6	7.3	0.4	1.8	3.025
2640	2.7	7.2	0.3	1.7	2.975
2641	2.8	7.1	0.2	1.6	2.925
2642	2.9	7	0.1	1.5	2.875
2643	3	6.9	6.94E-16	1.4	2.825
2644	3.1	6.8	-0.1	1.3	2.775
2645	3.2	6.7	-0.2	1.2	2.725
2646	3.3	6.6	-0.3	1.1	2.675
2647	3.4	6.5	-0.4	1	2.625
2648	3.5	6.4	-0.5	0.9	2.575
2649	3.6	6.3	-0.6	0.8	2.525
2650	3.7	6.2	-0.7	0.7	2.475
2651	3.8	6.1	-0.8	0.6	2.425
2652					

DH X DH Y DH Z

APPENDIX F: INSTITUTIONAL REVIEW BOARD APPROVAL FORM

Northern Michigan University

Memorandum

Office of Graduate Education and Research
1401 Presque Isle Avenue
Marquette, MI 49855-5301
906-227-2300
FAX: 906-227-2315
Web site: www.nmu.edu

TO: Samantha Wagner
Psychology Department

CC: Mounia Ziat
Psychology Department

DATE: June 18, 2013 (Approved May 30, 2013)

FROM: Brian Cherry, Ph.D.
Assistant Provost/IRB Administrator

SUBJECT: **IRB Proposal HS13-536**
IRB Approval Dates: 5/30/2013-5/30/2014**
Proposed Project Dates: 5/30/2013-5/30/2014
"A Study Comparing Healthy and Brain Damaged Individuals in a Virtual Environment with a Haptic Device"

The Institutional Review Board (IRB) has reviewed your proposal and has given it final approval. To maintain permission from the Federal government to use human subjects in research, certain reporting processes are required.

A. You must include the statement "Approved by IRB: Project # HS13-536" on all research materials you distribute, as well as on any correspondence concerning this project.

B. If a subject suffers an injury during research, or if there is an incident of non-compliance with IRB policies and procedures, you must take immediate action to assist the subject and notify the IRB chair (dereande@nmu.edu) and NMU's IRB administrator (bcherry@nmu.edu) within 48 hours. Additionally, you must complete an Unanticipated Problem or Adverse Event Form for Research Involving Human Subjects

C. Please remember that informed consent is a process beginning with a description of the project and insurance of participant understanding. Informed consent must continue throughout the project via a dialogue between the researcher and research participant.

D. If you find that modifications of methods or procedures are necessary, you must submit a Project Modification Form for Research Involving Human Subjects before collecting data.

E. **If you complete your project within 12 months from the date of your approval notification, you must submit a Project Completion Form for Research Involving Human Subjects. If you do not complete your project within 12 months from the date of your approval notification, you must submit a Project Renewal Form for Research Involving Human Subjects. You may apply for a one-year project renewal up to four times.

NOTE: Failure to submit a Project Completion Form or Project Renewal Form within 12 months from the date of your approval notification will result in a suspension of Human Subjects Research privileges <u>for all investigators listed on the application</u>, until the form is submitted and approved.

All forms can be found at the NMU Grants and Research website:
http://www.nmu.edu/grantsandresearch/node/102

ljc

APPENDIX G: CITI MODULE FOR HUMAN RESEARCH SUBJECTS

CITI Collaborative Institutional Training Initiative

Students Curriculum Completion Report
Printed on 8/25/2012

Learner: Samantha Wagner (username: srwagner1)
Institution: Northern Michigan University
Contact Information
718 1st Ave NW
Faribault, MN 55021
Department: Psychology
Phone: (906) 227-2935
Email: srwagner1@gmail.com

Student Researchers:

Stage 1. Basic Course Passed on 08/25/12 (Ref # 8505673)

Required Modules	Date Completed	Score
Students in Research	08/25/12	9/10 (90%)

For this Completion Report to be valid, the learner listed above must be affiliated with a CITI participating institution. Falsified information and unauthorized use of the CITI course site is unethical, and may be considered scientific misconduct by your institution.

Paul Braunschweiger Ph.D.
Professor, University of Miami
Director Office of Research Education
CITI Course Coordinator

Return